Experiments in nearly homogenous turbulent shear flow with a uniform mean temperature gradient. Part 1

By STAVROS TAVOULARIS† AND STANLEY CORRSIN

Department of Chemical Engineering,
The Johns Hopkins University, Baltimore, Maryland 21218

A reasonably uniform mean temperature gradient has been superimposed upon a nearly homogeneous turbulent shear flow in a wind tunnel. The overheat is small enough to have negligible effect on the turbulence. Away from the wind-tunnel entrance, the transverse statistical homogeneity is good and the temperature fluctuations and their integral scales grow monotonically like the corresponding velocity fluctuations (Harris, Graham & Corrsin 1977). Measurements of several moments, one- and two-point correlation functions, spectra, integral scales, microscales, probability densities, and joint probability densities of the turbulent velocities, temperature fluctuations, and temperature–velocity products are reported. The heat-transport characteristics are much like those of momentum transport, with the turbulent Prandtl number nearly 1. The temperature fluctuation is better correlated with the streamwise than the transverse velocity component, and the cross-component D_{12} of the turbulent diffusivity tensor has sign opposite to and about twice the magnitude of the diagonal component D_{22}. Some resemblance of directional properties (relative magnitudes of correlation functions, integral scales, microscales) of the temperature with those of the streamwise velocity is also observed. Comparisons of the present data with measurements in the inner part of a heated boundary layer and a fully turbulent pipe flow ($x_2/d = 0.25$) show comparable magnitudes of temperature–velocity correlation coefficients, turbulent Prandtl numbers and ratios of turbulent diffusivities, and show similar shapes of two-point correlation functions.

1. Introduction

The concept of homogeneous turbulence sheared by a uniform mean velocity gradient was introduced by von Kármán (1937) as a problem of complexity intermediate between unsheared homogeneous turbulence and rectilinear non-homogeneous shear flows. Indeed, in the absence of the complicating effects of rigid boundaries, turbulent/non-turbulent interfaces, and various types of inhomogeneities, this flow allows relatively simple analytical representation, although it is more difficult to realize experimentally than are the traditional shear flows such as channel and jet. It retains many of the crucial features of the more general sheared turbulent flows, so it can give physical insight into a variety of processes and can be useful in tests of some theories.

† Present address: Department of Mechanical Engineering, University of Ottawa, Ottawa, Canada K1N 6N5.

Some mathematical aspects of an exactly homogeneous turbulent shear flow were studied first by Reis (1952), Burgers & Mitchner (1953), and Craya (1958), all of whom derived equations for the two-point velocity correlations and the energy spectra. The idea remained an abstraction, however, because the most obvious method of trying to generate it, a 'turbulent rectilinear Couette flow', will not work; the integral scale of such a flow driven by a moving wall could not be much smaller than the gap between the walls, so no good approximation to homogeneity would result (Robertson 1959; Robertson & Johnson 1970).

The idea that a nearly homogeneous turbulent shear flow could actually be generated in the laboratory, and suggestions for its generation, were offered by Corrsin (1963). The first moderately successful experimental realization of such flows was achieved by Rose (1966) with the use of a plane grid with parallel rods of uniform diameter but non-uniform spacing. The resulting flow had reasonably uniform mean strain rate (about $13 \cdot 7$ s^{-1}) as well as nearly homogeneous transverse distributions of turbulent intensities and shear stress, but quite non-uniform transverse profiles of the integral length scales and Taylor microscales, because of the non-uniform rod spacing.

Other techniques used to produce nearly uniform mean shear and improved transverse homogeneity included a set of equal-width parallel channels with variable internal resistances (throttles) (Champagne, Harris & Corrsin 1970), combinations of uniform grids and a honeycomb of variable cross-section (Rose 1970; Hwang 1971) and a combination of non-uniform grid and a uniform honeycomb (Mulhearn & Luxton 1970, 1975). A number of conclusions were reached by these investigators: the turbulent shear-stress correlation coefficient approached an asymptotic value roughly equal to $0 \cdot 45$; the integral length scales and Taylor microscales increased indefinitely; the velocity correlation function and spectra reached approximately self-preserving forms; paradoxically (with the exception of the far-downstream region in the experiment of Mulhearn & Luxton 1970), the kinetic energy decreased from its initially imposed level to a seemingly asymptotic constant value, despite the expected positive net energy production associated with growing integral scales. Champagne *et al.* (1970) attributed this paradoxical result to the insufficiently long development time of the above flows, which can also be interpreted as a too small value of the total strain. Indeed, in the subsequent experiments of Harris *et al.* (1977), where the mean strain rate was roughly four times that of the previous experiments, with correspondingly larger mean strain, the turbulent kinetic energy passed through a minimum and then increased monotonically. They confirmed the continuous increase of the integral length scales, but found that the Taylor microscale increased more slowly than the integral scale, if at all.

In the earlier experiments, measurements have been made of the downstream development of the turbulent velocity components, as well as of some terms in the turbulent energy balance equation. Other measurements included velocity spectra, Eulerian integral length scales, Taylor microscales, and two-point space and space–time correlations, and iso-correlation contours of the velocity components and the shear stress in a fixed frame as well as in a frame following the mean motion.

The present report is centred about the study of the transport of heat as a passive scalar in a wind-tunnel turbulent flow with uniform mean velocity gradient, uniform mean temperature gradient, and transversely nearly homogeneous velocity and temperature fluctuation fields. No previous experiments in such a flow have ever been

reported; however, heat has often been used as a scalar contaminant in the study of turbulent transport and mixing in other 'simple' turbulent flows. The present study is a direct generalization of Wiskind's (1962) heat-transfer experiments in grid-generated isotropic turbulence with a uniform mean temperature gradient. He found that, consistent with the theoretical predictions of Corrsin (1952), the temperature fluctuation level far downstream of the grid appeared to reach a constant asymptotic value. Measurements in similar flows have also been reported by Alexopoulos & Keffer (1971) (their main objective was, however, the study of the interaction of this flow with a turbulent wake), and by Venkataramani & Chevray (1978), who conducted extensive measurements of probability and joint probability densities of velocity and temperature.

This report presents measurements of the general development of the velocity and temperature fluctuation fields and their characteristic scales, correlation functions, energy spectra, and probability densities of the two fields. Balances of the turbulent energy and the mean-square thermal fluctuations are attempted, and a number of dimensionless parameters characterizing momentum and heat transfer are evaluated from the data. A second report will focus on the fine structure of the two fields.

2. Analytical considerations

2.1. *The velocity field*

The instantaneous local velocity U_i in a viscous, incompressible flow field in the absence of body forces is customarily described by the Navier–Stokes equations. Decomposing the instantaneous values into temporal, spatial or ensemble averages (here denoted by overbars) and mean-free fluctuations (here denoted as lower-case letters), and following Reynolds' (1894) procedure, it is possible to derive balance equations for various moments of velocity, vorticity, etc. The simplified form of such equations in the case of homogeneous turbulent shear flow was given by Reis (1952), Burgers & Mitchner (1953) and Craya (1958). Extensive discussion, taking into consideration the experimental evidence, can be found in the papers by Champagne *et al.* (1970) and Harris *et al.* (1977).

The assumption employed in the latter two studies was that there exists a flow region with (*a*) two-dimensional, steady, rectilinear mean velocity $\overline{U}_1$ with a uniform mean gradient $\partial \overline{U}_1 / \partial x_2$; (*b*) velocity and pressure fluctuations statistically homogeneous in any (x_2, x_3) plane; and (*c*) all mean values stationary with respect to a 'laboratory' inertial frame.

As a direct consequence of the above assumptions, the mean continuity equation reduces to

$$\partial \overline{U}_1 / \partial x_1 = 0; \tag{1}$$

therefore $\overline{U}_1$ is a function of x_2 only. On the other hand, the equation for the mean turbulent kinetic energy $\overline{q^2} \equiv \overline{u_i u_i}$ becomes (after the omission of higher-order terms)

$$\overline{U}_1 \frac{d(\tfrac{1}{2}\overline{q^2})}{dx_1} \approx -\overline{u_1 u_2} \frac{d\overline{U}_1}{dx_2} - \epsilon, \tag{2}$$

where

$$\epsilon \equiv \nu \overline{\frac{\partial u_i}{\partial x_k} \left(\frac{\partial u_i}{\partial x_k} + \frac{\partial u_k}{\partial x_i} \right)}$$

is the mean turbulent energy dissipation rate. Equation (2) is inconsistent with the hopes for formal transverse homogeneity, since its left side is a function of x_2 while its right side is not. Thus, transverse homogeneity is theoretically impossible. In the present experiment, fortunately, all three assumptions are approximately satisfied (see Harris *et al.* 1977).

2.2. *The temperature field*

The temperature T at a point in a fluid with constant molecular diffusivity γ obeys the equation

$$\frac{\partial T}{\partial t} + U_i \frac{\partial T}{\partial x_i} = \gamma \frac{\partial^2 T}{\partial x_i \partial x_i}. \tag{3}$$

Decomposing T into mean $\bar{T}$ and fluctuation θ, it is possible to derive balance equations for the various temperature moments and, in combination with the Navier–Stokes equations, for the temperature–velocity covariances.

Assume a velocity field approximately satisfying assumptions (*a*), (*b*), and (*c*) above. In addition, assume a superimposed passive temperature field with the following properties: (*d*) two-dimensional, linear mean temperature profile,

$$\frac{\partial \bar{T}}{\partial x_2} = \text{const.}, \quad \text{independent of } x_2, x_3, \quad \frac{\partial \bar{T}}{\partial x_3} = 0;$$

(*e*) fluctuations statistically homogeneous on any (x_2, x_3) plane; and (*f*) stationary.

In the absence of an equation analogous to (1) there is no *a priori* restriction that $\partial \bar{T}/\partial x_1$ should vanish. Indeed, the balance equation for the mean temperature (Kampé de Feriet 1937) reduces to

$$\frac{\partial}{\partial x_1} \left(\bar{U}_1 \bar{T} + \overline{\theta u_1} - \gamma \frac{\partial \bar{T}}{\partial x_1} \right) = 0, \tag{4}$$

or

$$\bar{U}_1 \bar{T} + \overline{\theta u_1} - \gamma \frac{\partial \bar{T}}{\partial x_1} = fn(x_2). \tag{4a}$$

The additional assumption that (*g*) $\partial \bar{T}/\partial x_1 \approx 0$ would yield

$$\overline{\theta u_1} \approx \text{const.}$$

asymptotically throughout the flow. In view of the measured downstream increase of $\overline{u_1^2}$ and $\overline{\theta^2}$, the correlation coefficient $\overline{\theta u_1}/\theta' u_1'$ would vanish asymptotically. Measurements (§4) show, however, that this correlation coefficient retained a relatively high value (roughly 0·6) in the entire test volume; yet assumption (*g*) was (also experimentally) found to be well approximated in the same test volume.

With assumptions (*a*)–(*g*), the equation for the balance of $\overline{\theta^2}$ (Corrsin 1952) reduces to

$$\bar{U}_1(x_2) \frac{d(\frac{1}{2}\overline{\theta^2})}{dx_1} \approx -\overline{\theta u_2} \frac{d\bar{T}}{dx_2} - \frac{1}{2} \frac{d(\overline{\theta^2 u_1})}{dx_1} + \frac{1}{2}\gamma \frac{d^2\overline{\theta^2}}{dx_1^2} - \gamma \overline{\frac{\partial \theta}{\partial x_i} \frac{\partial \theta}{\partial x_i}}. \tag{5}$$

As in the case of the turbulent energy equation, an inconsistency with transverse homogeneity occurs, since the left-hand side of equation (5) depends on x_2, while the
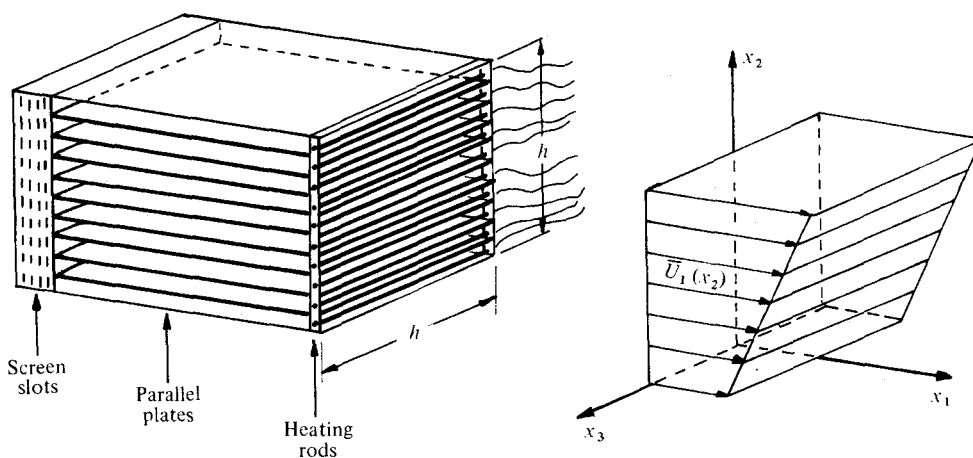
FIGURE 1. Sketch of the shear generator and heating system.

right-hand side does not if the fluctuations are assumed to be transversely homogeneous. Omitting negligible terms, equation (5) reduces to

$$\overline{U}_1 \frac{d(\frac{1}{2}\overline{\theta^2})}{dx_1} \approx -\overline{\theta u_2} \frac{d\overline{T}}{dx_2} - \chi, \tag{6}$$

where $\chi \equiv \gamma \overline{(\partial \theta / \partial x_i)(\partial \theta / \partial x_i)}$ is the temperature fluctuation dissipation rate.

The equations for one-point temperature–velocity covariances (Corrsin 1953) take the special forms

$$\overline{U}_1 \frac{d\overline{\theta u_1}}{dx_1} \approx -\overline{\theta u_2} \frac{d\overline{U}_1}{dx_2} - \overline{u_1 u_2} \frac{d\overline{T}}{dx_2} - \frac{d\overline{\theta u_1^2}}{dx_1} - \frac{1}{\rho} \overline{\theta \frac{\partial P}{\partial x_1}} - (\gamma + \nu) \overline{\frac{\partial u_1}{\partial x_i} \frac{\partial \theta}{\partial x_i}}, \tag{7}$$

$$\overline{U}_1 \frac{d\overline{\theta u_2}}{dx_1} \approx -\overline{u_2^2} \frac{d\overline{T}}{dx_2} - \frac{d\overline{\theta u_1 u_2}}{dx_1} - \frac{1}{\rho} \overline{\theta \frac{\partial P}{\partial x_2}} - (\gamma + \nu) \overline{\frac{\partial u_2}{\partial x_i} \frac{\partial \theta}{\partial x_i}}. \tag{8}$$

The equation for θu_3 reduces to $0 = 0$ by symmetry.

3. Experimental facilities and instrumentation

The wind tunnel used for the experiments of Rose (1966), Champagne *et al.* (1970), and Harris *et al.* (1977) was also used in the present investigation; an essentially constant mean pressure over the test section was attained by adjusting the vertical walls. The shear-turbulence generator used by Harris *et al.* (1977) was modified by replacing the exit turbulence-generating rods with heating rods. The generator (figure 1) consisted of a set of ten† parallel channels, 2·76 cm wide and 61 cm long, separated by aluminium plates of thickness 0·318 cm. The mean speed in each channel was adjusted with (throttle) screens of various mesh sizes inserted in slots near the upstream end.

† The shear-flow generators used in the experiments of Champagne *et al.* (1970) and Harris *et al.* (1977) also consisted of ten parallel channels and not twelve, as mentioned by mistake in these two papers.

The original 0.318×0.318 cm square rods at the channel exits were replaced by round heating rods (Chromalox TSSM 14XX, special order) of diameter 0.508 cm and resistance 25 ohm. The conventional grid solidity (i.e. the ratio of the projected cross-sections of the rods and plates over the total tunnel cross-section) was thus increased from 0.206 to 0.268. Of course the effective solidity is higher due to the thickness of the boundary layers on the separating plates. In any case, the change of grid solidity was in the correct direction for minimizing turbulence field changes (compared with the data of Harris *et al.*), because the wake behind a square rod is wider than that behind a round rod of equal projected area. Another favourable indication was that the turbulent intensity produced by a square-mesh, square-rod grid of solidity 0.206 was roughly equal to that produced by a square-mesh, round-rod grid of solidity 0.268 (Corrsin 1963, figure 6; the curves were linearly extrapolated to lower solidities). The rods were heated by the 110 volt a.c. power line through individual variable trans-formers. To minimize the effect of heat losses through the top wall of the test section, two silicone-rubber, flexible heaters (Electroflex Heat Inc., with thickness approxi-mately 0.15 cm and rectangular areas 28×30.5 cm and 30.5×30.5 cm, glued on aluminium sheets 0.08 cm thick) were fastened on the inner side of the tunnel top; the temperature of these heaters was adjusted to match the desired local mean temperature of the flow.

Hot-wires powered by constant-temperature anemometers (DISA 55D01) were used as velocity transducers. The streamwise velocity was measured with a $5 \, \mu$m diameter, 1.2 mm long, tungsten wire (DISA 55P11), while the transverse components were measured with a tungsten X-wire probe (DISA 55P51) with wires $5 \, \mu$m diameter, 1.2 mm long, and 1.0 mm apart. For the transverse derivatives of the streamwise velocity, a parallel wire probe (DISA 55P71) with wires $2.5 \, \mu$m diameter, 1.2 mm long, and 0.5 mm apart was used. The mean temperature and the reference tempera-ture upstream of the heating system were monitored with two glass-coated thermistor miniprobes (Fenwal GC32M21). The fluctuating temperature was measured with a $1 \, \mu$m diameter, 0.4 mm long platinum 'cold' wire (DISA 55P31), operated at a con-stant current 0.25 mA with the use of a home-made electronic circuit (Tavoularis 1978a). A second 'cold' wire (home-made), $0.6 \, \mu$m diameter, and 0.8 mm long, was placed about 0.6 mm from the DISA cold-wire when the transverse temperature de-rivatives were measured. The velocity sensitivity of the cold wires was measured and found to be negligible, while their frequency response to temperature fluctuations was estimated to be fairly flat up to 3 kHz for the $1 \, \mu$m wire and up to 5 kHz for the $0.6 \, \mu$m wire (-3 dB points), according to La Rue, Deaton & Gibson (1975) and Højstrup, Rasmussen & Larsen (1976). A PDP 11/40 digital minicomputer allowed discrete data acquisition and processing. Details of instrumentation and experimental procedures and accuracies can be found in the dissertation of Tavoularis (1978b).

4. The measurements

4.1. *A preliminary study of the heating effects*

A study of the temperature field produced by a single heating rod was performed first, as an initial test of the temperature-measuring system, to serve as a guide for the final adjustment of the mean temperature gradient, and because of its possible intrinsic
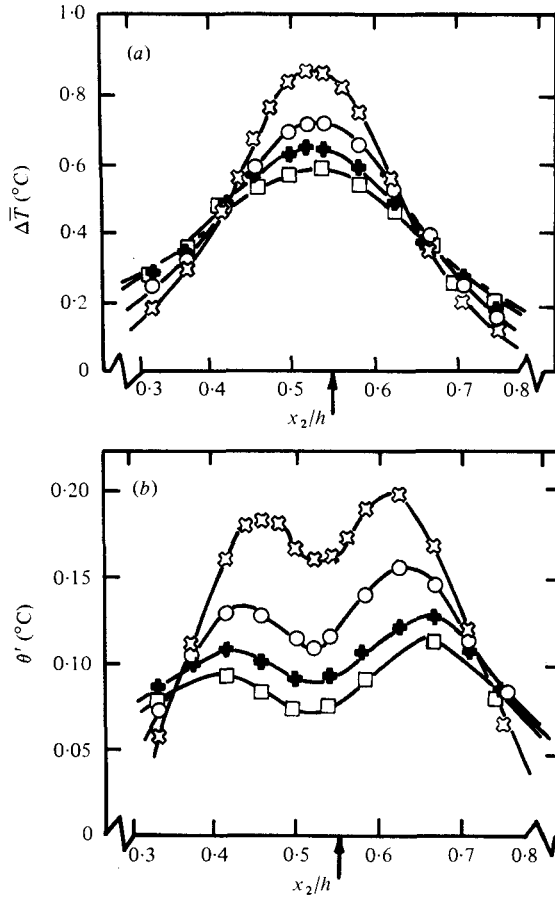
FIGURE 2. Temperature field of rod number 5: (*a*) the mean temperature rise, (*b*) the r.m.s. temperature fluctuations. ✩, $x_1/h = 5.0$; ◯, $x_1/h = 7.5$; ✧, $x_1/h = 9.5$; ▢, $x_1/h = 11.0$. The arrows indicate location of the heated rod.

interest. For this purpose, rod number 5, whose axis was positioned at $x_2/h = 0.55$ (see figure 1 for an explanation of the symbols), was the only one heated. The downstream development of the resulting vertical profiles of the mean temperature rise $\Delta \bar{T}$ ($\equiv \bar{T} - T_a$; T_a is the flow temperature upstream of the shear-flow generator) and the r.m.s. temperature fluctuation θ' are shown in figure 2. The expected slight asymmetry due to mean shear is observed in both sets of profiles. The downstream decrease of the maximum temperature rise $\Delta \bar{T}_{max}$ is shown in figure 3, together with a family of isotherms in the vertical centre-plane of the tunnel.

4.2. *Development of the velocity and temperature fields*

The velocity field was essentially the same as the one of Harris *et al.* (1977). Several measurements were repeated in order to test the effects of the system modifications, ageing of the apparatus, and differences in measuring techniques. The present (digital) techniques are presumably more reliable than those used in the earlier study. Since the heating effect on the velocity field was negligible (see § 5.1), all velocity measurements
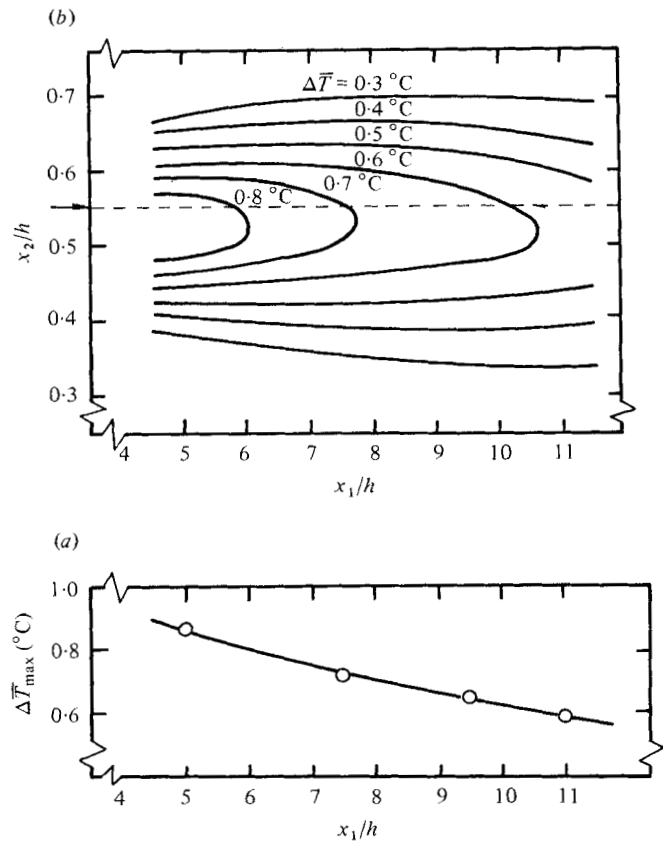
FIGURE 3. Temperature field of rod number 5: (a) downstream development of the maximum temperature rise; (b) isotherms in the vertical centre-plane of the tunnel. The arrow indicates location of the heated rod.
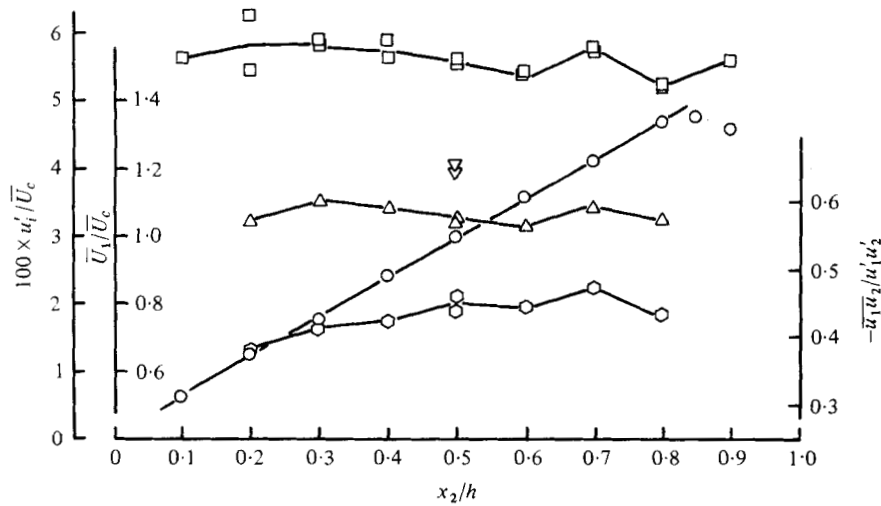

FIGURE 4. Mean velocity, turbulent intensities, and shear-stress correlation coefficient profiles $(x_1/h = 11\cdot0)$. $\bigcirc$, $\overline{U}_1/\overline{U}_c$; $\square$, $u_1'/\overline{U}_c$; $\triangle$, $u_2'/\overline{U}_c$; ∇, $u_3'/\overline{U}_c$; $\mathbf{O}$, $-\overline{u_1 u_2}/u_1' u_2'$.
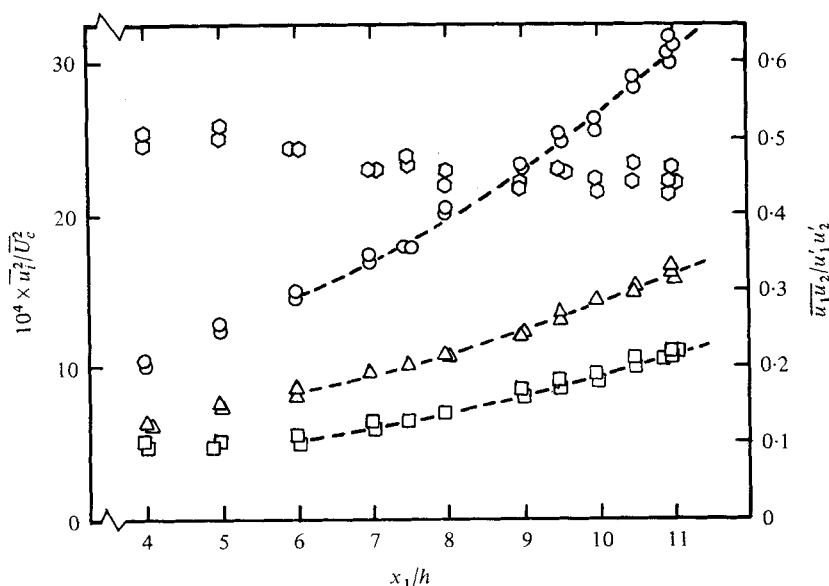
FIGURE 5. Downstream development of turbulence component energies and shear-stress correlation coefficient. $\bigcirc$, $\overline{u_1^2}/\overline{U}_c^2$; $\square$, $\overline{u_2^2}/\overline{U}_c^2$; $\triangle$, $\overline{u_3^2}/\overline{U}_c^2$; $\mathbf{O}$, $-\overline{u_1 u_2}/u_1' u_2'$; — — —, fitted parabolae.
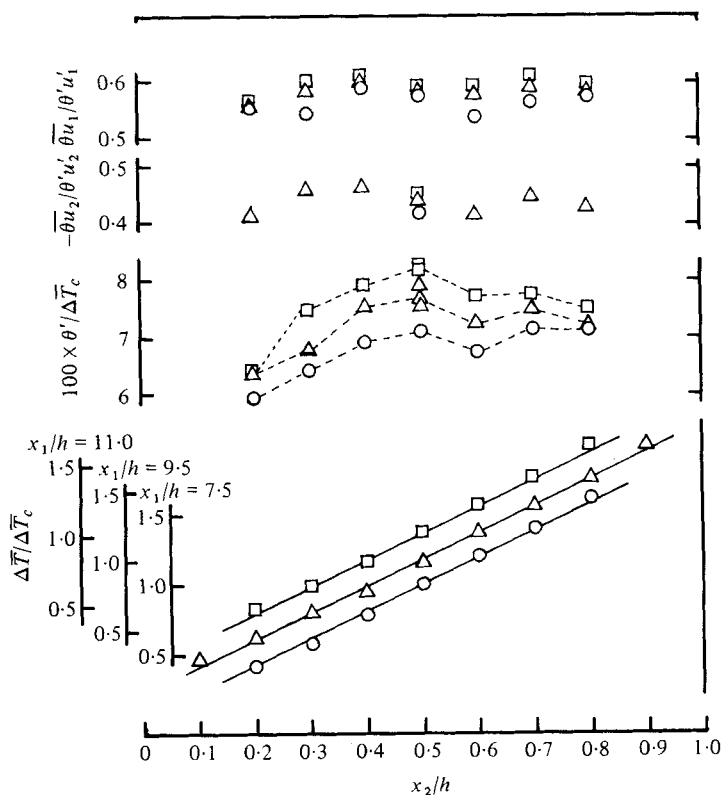

FIGURE 6. Vertical profiles of the mean temperature rise, the r.m.s. temperature fluctuations, and the heat transport correlation coefficients. $\bigcirc$, $x_1/h = 7.5$; $\triangle$, $x_1/h = 9.5$; $\square$, $x_1/h = 11.0$.
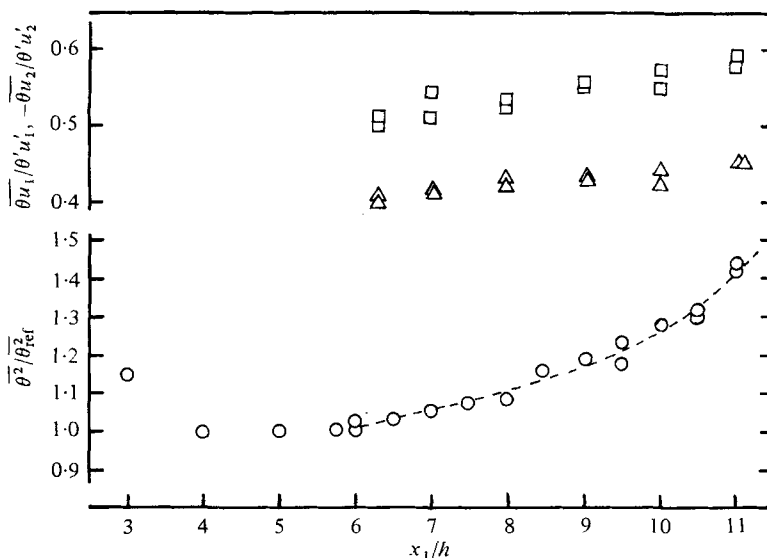
FIGURE 7. Downstream development of the mean squared temperature fluctuations and the heat-transport correlation coefficients. $\bigcirc$, $\overline{\theta^2}/\overline{\theta^2_{\mathrm{ref}}}$; $\overline{\theta^2_{\mathrm{ref}}} \approx 0\cdot011$ °C^2; – – –, fitted cubic polynomial; $\square$, $\overline{\theta u_1}/\theta' u_1'$; $\triangle$, $-\overline{\theta u_2}/\theta' u_2'$.

were performed in the unheated flow, so that the hot-wire signals were free of fluctuating temperature contamination. Corrections for slow mean ambient temperature drift, measured with a thermistor positioned close to the hot-wire, were applied to the signals.

The mean velocity profiles in the vertical centre-plane ($x_3/h = 0\cdot0$) at three downstream stations, $x_1/h = 7\cdot5$, $9\cdot5$, and $11\cdot0$, were practically indistinguishable from each other and presented excellent linearity for $0\cdot1 < x_2/h < 0\cdot8$. The straight lines fitted to the experimental points had a slope $d\overline{U}_1/dx_1 = 46\cdot8$ s^{-1}, which was $2\cdot5$ % lower than that during most of the measurements of Harris et al. Uniformity of $d\overline{U}_1/dx_2$ in the x_3 direction was not checked independently, but agreement within 3 % among the values at $x_3/h = 0\cdot0$, $0\cdot25$, and $-0\cdot25$ was reported by Harris et al. The centre-plane speed $\overline{U}_c$ was $12\cdot4$ m s^{-1}, equal to that during most of the earlier measurements.

Figure 4 shows vertical profiles of the mean velocity, the r.m.s. turbulent velocities, and the shear-stress correlation coefficient at $x_1/h = 11\cdot0$. Similar profiles at $x_1/h = 7\cdot5$ and $9\cdot5$ presented slightly higher scatter but smaller wall effects. The downstream development of the mean squared turbulent velocities and the shear-stress correlation on the centre-line of the tunnel is shown in figure 5. The mean squared velocities were fitted by least-squares parabolas for convenience in later calculations. This choice of fitted polynomial agrees well with the present measurements, although contradicted by some rough theoretical arguments by Harris et al., who predicted an asymptotically linear increase of turbulent kinetic energy.

The mean temperature profiles at three downstream stations are shown in figure 6. The fitted straight lines, having a slope $d\overline{T}/dx_2 = 9\cdot5$ °C m^{-1}, demonstrate the good linearity and downstream constancy† of the mean temperature gradient for $x_1/h > 7\cdot5$

† Recall that, unlike the velocity case, this constancy is not inferred a priori from the simplified balance equations.

$$\overline{u_1^3}/u_1'^3 = -0.22 \qquad \overline{\theta^3}/\theta'^3 = 0.00$$
$$\overline{u_2^3}/u_2'^3 = 0.16 \qquad \overline{\theta^4}/\theta'^4 = 3.0$$
$$\overline{u_3^3}/u_3'^3 = 0.00 \qquad \overline{\theta u_1}/\theta' u_1' = 0.59$$
$$\overline{u_1^4}/u_1'^4 = 3.1 \qquad \overline{\theta u_2}/\theta' u_2' = -0.45$$
$$\overline{u_2^4}/u_2'^4 = 3.2 \qquad \overline{\theta^2 u_1}/\theta'^2 u_1' = -0.05$$
$$\overline{u_3^4}/u_3'^4 = 3.3 \qquad \overline{\theta^2 u_2}/\theta'^2 u_2' = 0.06$$
$$\overline{u_1 u_2}/u_1' u_2' = -0.45 \qquad \overline{\theta u_1^2}/\theta' u_1'^2 = -0.10$$
$$\overline{u_1^2 u_2}/u_1'^2 u_2' = 0.13 \qquad \overline{\theta u_2^2}/\theta' u_2'^2 = -0.12$$
$$\overline{u_1 u_2^2}/u_1' u_2'^2 = -0.18$$

TABLE 1. One-point moments and correlations ($x_1/h = 11.0$).

and $0.2 < x_2/h < 0.8$. The centre-line temperature rise $\Delta \overline{T_c}$ was constant (about $1.5\ °\text{C}$) in the test section and low enough to guarantee negligible buoyancy effects on the velocity field.

Figure 6 gives profiles of the r.m.s. temperature fluctuations and of the temperature–velocity correlation coefficients in the vertical centre-plane of the tunnel. The degree of transverse homogeneity of θ' is comparable to that of the r.m.s. turbulent velocities for $0.3 < x_2/h < 0.8$. The correlation coefficient profiles show better uniformity than those of θ' and u_i', due to the inherent normalization.

The downstream development of the centre-line $\overline{\theta^2}$, $\overline{\theta u_1}/\theta' u_1'$, and $\overline{\theta u_2}/\theta' u_2'$ is in figure 7. For $x_1/h < 4$, decay of the initial temperature fluctuations exceeds production, but farther downstream a monotonic increase in $\overline{\theta^2}$ takes place. $\overline{\theta^2}$ was normalized with $\overline{\theta_{\text{ref}}^2} \approx 0.011\ °\text{C}^2$, measured with a cold-wire held fixed at $x_1/h = 5.75$. Variations in $\overline{\theta_{\text{ref}}^2}$, attributable mainly to line voltage fluctuations, were about $\pm 5\%$. The $\pm 3\%$ scatter in $\overline{\theta^2}/\overline{\theta_{\text{ref}}^2}$ reflects mainly the finite sampling interval errors. For convenience, the data in the range $6.0 < x_1/h < 11.0$ were fitted with a least squares cubic polynomial. Both correlation coefficient magnitudes increase slightly downstream. The shear correlation coefficient decreases slightly over the same range.

4.3. *One-point moments and correlations*

Typical values of the skewness and flatness factors of the three turbulent velocities and temperature, measured on the centre-line of the tunnel at $x_1/h = 11.0$, are given in table 1. Mixed moments are included.

The systematic errors involved in these measurements (due to electronic noise, mixed velocity–temperature sensitivities and possible calibration inaccuracies) were estimated to be much smaller than the random experimental errors (due to finite sampling intervals, slight changes in the wind tunnel speed, and other unpredictable sources). Typical values of the random errors, expressed as standard deviations of an ensemble of measurement, were 0.03 for the skewness factors and 0.05 for the flatness factors.

All flatness factors are close to 3.0, the value for a normal random variable. However, some non-normal behaviour of u_1 and u_2 is demonstrated by the non-zero values of their skewnesses.

The negative sign of the skewness of u_1 may be a consequence of the downstream increase in $\overline{u_1^2}$. Negative values of u_1 (coming with fluid from positions with higher x_1) tend to have larger amplitudes than do positive values of u_1; since, by definition,
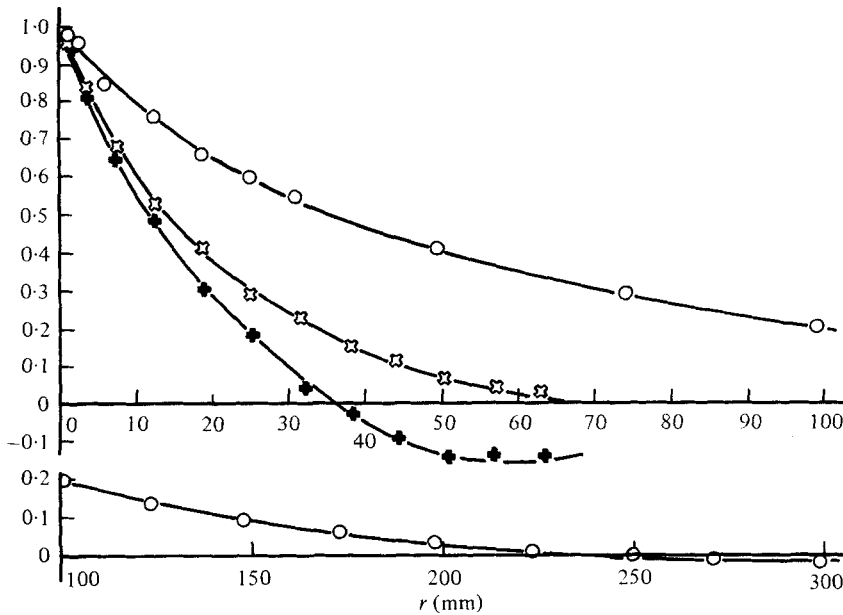
FIGURE 8. Streamwise turbulent velocity autocorrelation along the three co-ordinate axes.
$\bigcirc$, $R_{11}(r, 0, 0; 0)$; ✿, $R_{11}(0, r, 0; 0)$; $\blacklozenge$, $R_{11}(0, 0, r; 0)$.

$\bar{u}_1 = 0$, a negative $\overline{u_1^3}$ is produced. This argument was offered by Corrsin (1950) for the skewness of transverse velocity in a transversely inhomogeneous shear flow. Similarly, the skewness of u_2 may be attributable to the transverse inhomogeneity. The sign of $\partial \overline{u_2^2}/\partial x_2$ (figure 4) is appropriate, and the magnitude is about half of $\partial \overline{u_1^2}/\partial x_1$.

All three second-order mixed correlation coefficients, shown in table 1, are distinctly non-zero. At first glance, the near equality of $\overline{u_1 u_2}/u_1' u_2'$ and $\overline{\theta u_2}/\theta' u_2'$ might seem to support the ('Reynolds') analogy between momentum and heat transport, although the fact that $\overline{\theta u_1}/\theta' u_1'$ is higher in magnitude than $\overline{\theta u_2}/\theta' u_2'$ is a bit surprising since there is no mean temperature gradient along x_1. This topic will be further discussed (§§ 5.3 and 6.3). The third-order mixed correlation coefficients show small departures from zero; the highest magnitudes are those involving velocities only. Third-order correlations are, in general, subject to higher experimental errors.

4.4. Two-point correlations

The components of a Cartesian, two-point velocity fluctuation correlation coefficient tensor can be defined as

$$R_{ij}(r_1, r_2, r_3; \tau) \equiv \frac{\overline{u_i(\mathbf{x}; t)\, u_j(\mathbf{x} + \mathbf{r}; t + \tau)}}{\overline{u_i'(\mathbf{x})\, u_j'(\mathbf{x} + \mathbf{r})}}, \tag{9}$$

where homogeneity and stationarity have been assumed for the arguments of R_{ij}; R_{ij} is called an autocorrelation function when $i = j$, and a cross-correlation function when $i \neq j$. The temperature autocorrelation $R_{\theta\theta}$ and the temperature–velocity cross-correlation vector $R_{\theta u_i}$ are defined similarly.

Correlations along x_2 and x_3 were measured with two probes mounted on a traversing device with 130 mm maximum separation and 0.2 mm accuracy. To avoid the wake
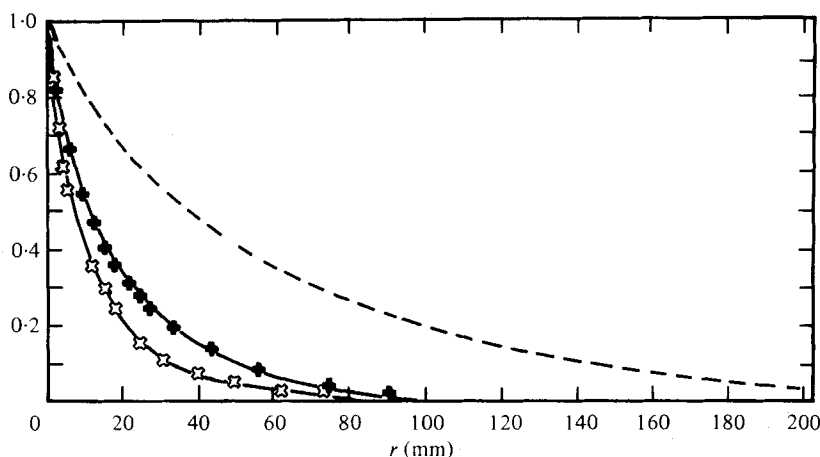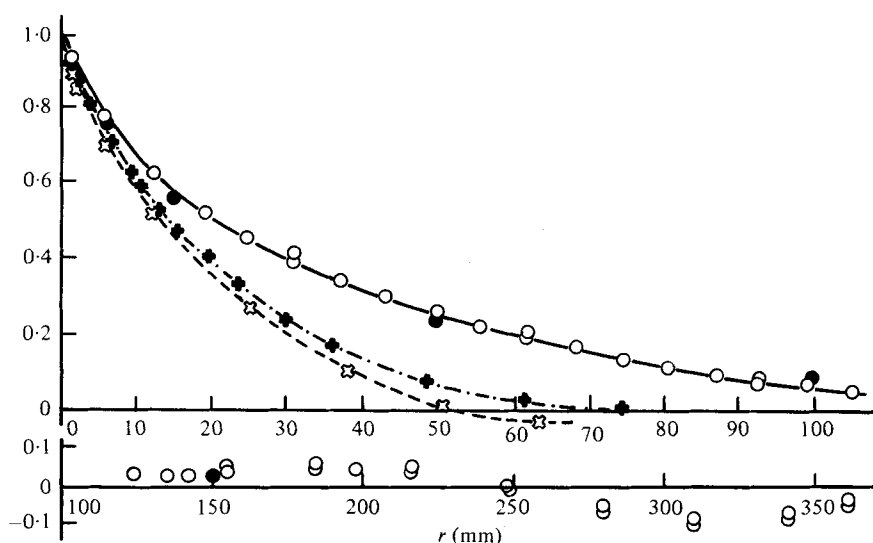
FIGURE 9. Autocorrelation of the turbulent velocities in the streamwise direction.
$---$, $R_{11}(r, 0, 0; 0)$; ✡, $R_{22}(r, 0, 0; 0)$; ✤, $R_{33}(r, 0, 0; 0)$.

FIGURE 10. Temperature autocorrelation along the three co-ordinate axes. ●,
$R_{\theta\theta}(r, 0, 0; 0)$; ○, $R_{\theta\theta}(0, 0, 0; r/\overline{U}_1)$; ✤, $R_{\theta\theta}(0, r, 0; 0)$; ✡, $R_{\theta\theta}(0, 0, r; 0)$.

of the upstream wire, small-separation regions of the correlations along the x_1 axis were measured by extrapolating to $r_3 = 0$ the corresponding $R(r_1, 0, r_3; 0)$ correlations. For separations larger than about 100 mm, the wake interference effect was found to be negligible (see also Champagne *et al.* 1970). Some correlations along x_1 were measured from temporal signal records of a single probe with the use of Taylor's 'frozen flow' approximation as

$$R(r, 0, 0; 0) \approx R(0, 0, 0; r/\overline{U}_1). \tag{10}$$

The validity of this approximation for $R_{\theta\theta}$ and $R_{\theta u_2}$ was confirmed by direct measurements (see figures 10 and 11); Champagne *et al.* (1970) confirmed equation (10) for the velocity correlations in the lower shear case.
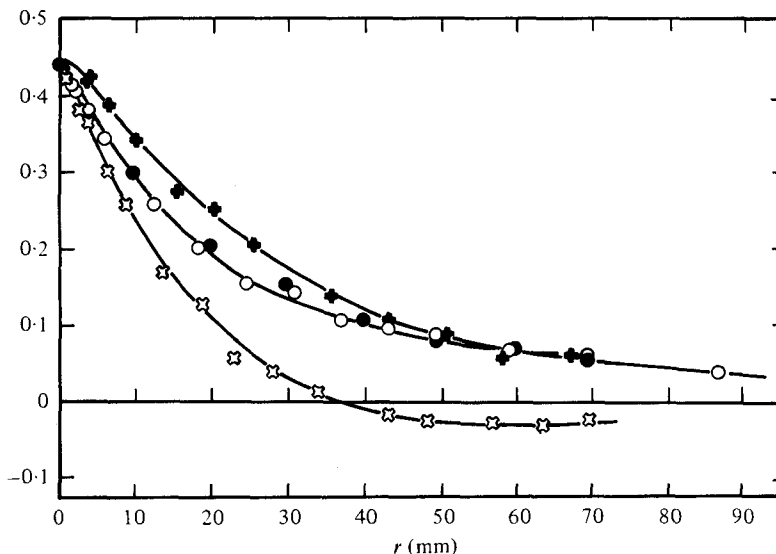
FIGURE 11. Temperature–transverse-velocity cross-correlation along the three co-ordinate axes.
●, $-R_{\theta u_2}(r, 0, 0; 0)$; ○, $-R_{\theta u_2}(0, 0, 0; r_1/\overline{U}_1)$; ✚, $-R_{\theta u_2}(0, r, 0; 0)$; ✿, $-R_{\theta u_2}(0, 0, r; 0)$.

Corrections for electronic noise and for velocity sensitivity of the cold-wire were applied to the measurements when necessary; they were at most 1 % of the maxima of the corresponding curves.

The streamwise velocity autocorrelations along the three Cartesian axes, shown in figure 8 (fixed probe on the centre-line, at $x_1/h = 11 \cdot 0$), are in good qualitative agreement with the data of Harris *et al.* (1977). Only $R_{11}(0, 0, r; 0)$ has a region of appreciable negative values. Figure 9 shows the autocorrelations of the three velocity components along the x_1 axis, at $x_1/h = 11 \cdot 0$, computed from single-probe time signals with the use of Taylor's approximation. None of these curves reaches a significant negative value over the r range covered.

The temperature autocorrelation curves along the three Cartesian axes are shown in figure 10 (fixed probe at $x_1/h = 11 \cdot 0$). The three functions are distinct (they would be equal in an isotropic field). Finally, the temperature–transverse-velocity cross-correlation coefficients along the same axes are shown in figure 11. Discussion about the above results will be given later, in § 6.2.

Harris *et al.* have presented isocorrelation contours for R_{11} and R_{12} in the (x_1, x_2) and (x_1, x_3) planes. Similar isocorrelation contours for $R_{\theta\theta}$ and $R_{\theta u_2}$ are shown in figure 12. The isocorrelation contours in the centre-plane parallel to the mean velocity gradient have a tilted oval shape, presumably due to the mean shear. In contrast, contours in the centre-plane perpendicular to the mean velocity gradient are roughly symmetric with respect to both r_1 and r_3.

The lines in figure 12 represent the 'best' families of similar ellipses fitted to the data. The isocorrelation contours are expected to attain elliptical shapes for

$$r \ll \lambda \quad (r^2 = r_1^2 + r_2^2 + r_3^2)$$

but not for higher r (for an example of a Taylor's expansion of the correlation coefficients producing elliptical contours at small r, see Champagne *et al.* 1970). The shapes
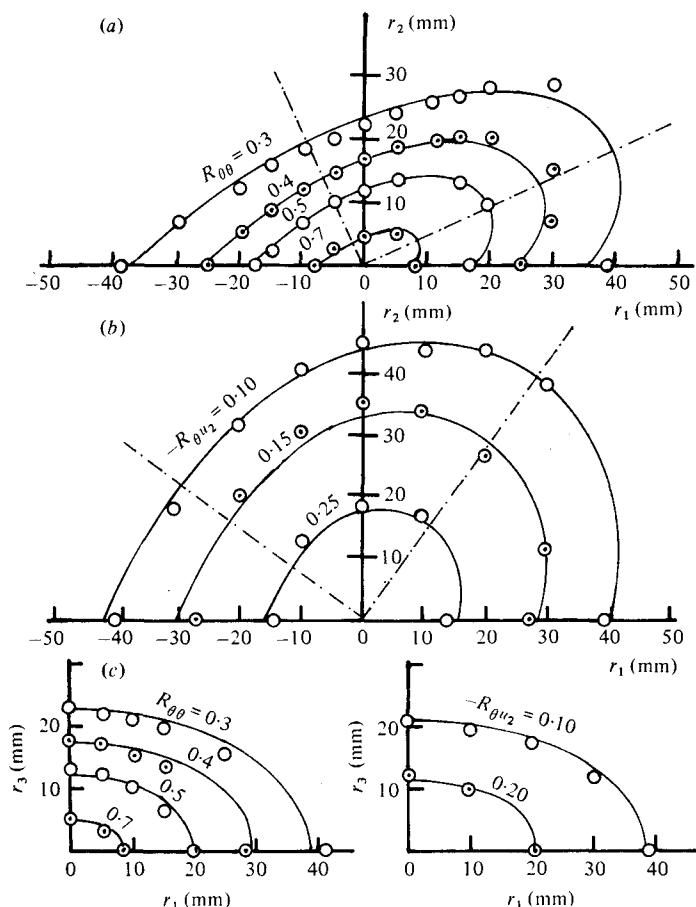
FIGURE 12. Isocorrelation contours (a) $R_{\theta\theta}(r_1, r_2, 0; 0)$, (b) $-R_{\theta u_2}(r_1, r_2, 0; 0)$, (c) $R_{\theta\theta}(r_1, 0, r_3; 0)$, (d) $-R_{\theta u_2}(r_1, 0, r_3; 0)$. The lines represent the optimal families of ellipses fitted to the data.

and orientations of the ellipse families are shown in table 2. The R_{11} and R_{12} contours were taken from Harris *et al.* (1977).

Streamwise space–time correlations for R_{11}, R_{22}, and R_{12} were measured by Harris *et al.* (1977). Figure 13 shows a typical family of temperature space–time correlations, measured with two wires separated in the streamwise direction. Marked with vertical lines on this figure are the times

$$\tau_c \equiv r/\overline{U}_c, \tag{11}$$

corresponding to the time required for a fluid particle travelling with the local mean speed to cover the distance between the two probes. The times τ_c almost coincide with the positions of the maxima of the corresponding correlations; a significant deviation is observed only for the largest probe separation, which, however, was obtained with the upstream probe positioned in the developing part of the flow. The envelope of the maxima of all correlations represents the temperature autocorrelation in a frame convected with the local mean speed. If Taylor's approximation were valid for large probe separations, this envelope would be a horizontal line.

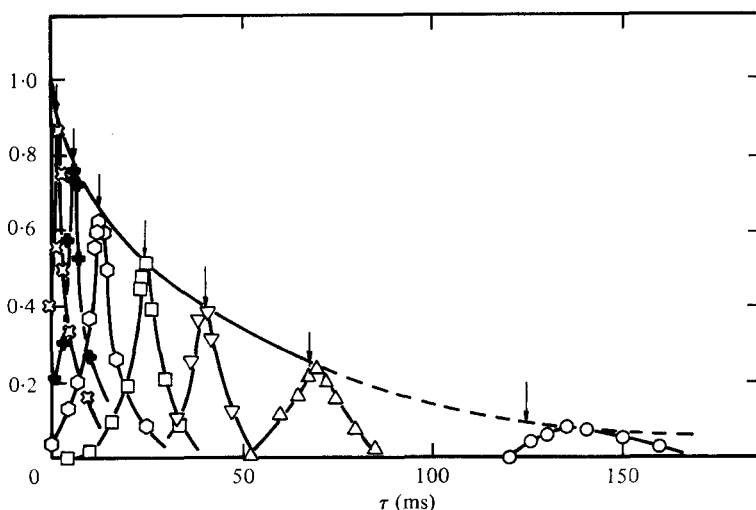| Contour	Axis ratio	Angle of major axis with x_1
$R_{\theta\theta}(r_1, r_2)$	2·0	25°
$R_{\theta\theta}(r_1, r_3)$	1·7	0°
$R_{\theta u_2}(r_1, r_2)$	1·3	54°
$R_{\theta u_2}(r_1, r_3)$	1·8	0°
$R_{11}(r_1, r_2)$	2·6	13°
$R_{11}(r_1, r_3)$	2·7	0°
$R_{12}(r_1, r_2)$	3·4	16°

TABLE 2

FIGURE 13. Temperature space–time correlations in the streamwise direction. ⊠, $r = 25$ mm; ✚, $r = 75$ mm; ◯, $r = 150$ mm; ▢, $r = 300$ mm; ▽, $r = 500$ mm; △, $r = 835$ mm; ◯, $r = 1555$ mm. The vertical arrows indicate the corresponding times $\tau_c = r/\overline{U}_c$.

4.5. One-dimensional frequency spectra

Spectra were measured with a digital harmonic analysis technique; details are given by Tavoularis (1978b). Corrections were applied for electronic noise and for velocity sensitivity of the temperature wire when necessary. The spectra have not been corrected for wire-length errors and separation, but Wyngaard's (1968, 1969, 1971) estimates of these errors for the power spectra of the velocity and temperature fluctuations are included in the appropriate figures. No such estimates are available for cross-spectra; for this reason, cross-spectra are presented up to only about 3 kHz ($\approx 0.25 f_K$; $f_K \equiv \overline{U}_1(\epsilon/\nu^3)^{\frac{1}{4}}/2\pi$ is the convected passing frequency of the Kolmogoroff microscale), where the wire length errors are, presumably, small. Errors due to differences in the time constants of the hot and cold wires (see Mestayer & Chambaud 1979) were effectively reduced by low-pass filtering the signals to 3 kHz; all sensors are expected to have good frequency response in this bandwidth.

The one-dimensional frequency spectra $F_{11}(f)$ of u_1 at three downstream stations along the tunnel centre-line are shown in figure 14. The values of $F_{11}(f)$ at all frequencies increase downstream, corresponding to the increase of the turbulent kinetic energy and

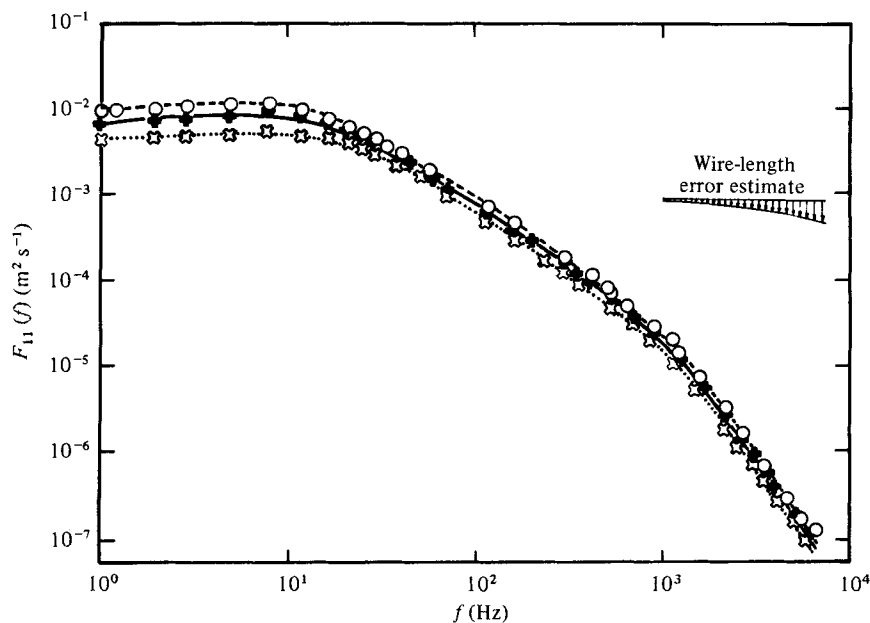FIGURE 14. One-dimensional spectra of the streamwise turbulent velocity.
$\odot$, $x_1/h = 7.5$; $\clubsuit$, $x_1/h = 9.5$; $\bigcirc$, $x_1/h = 11.0$.
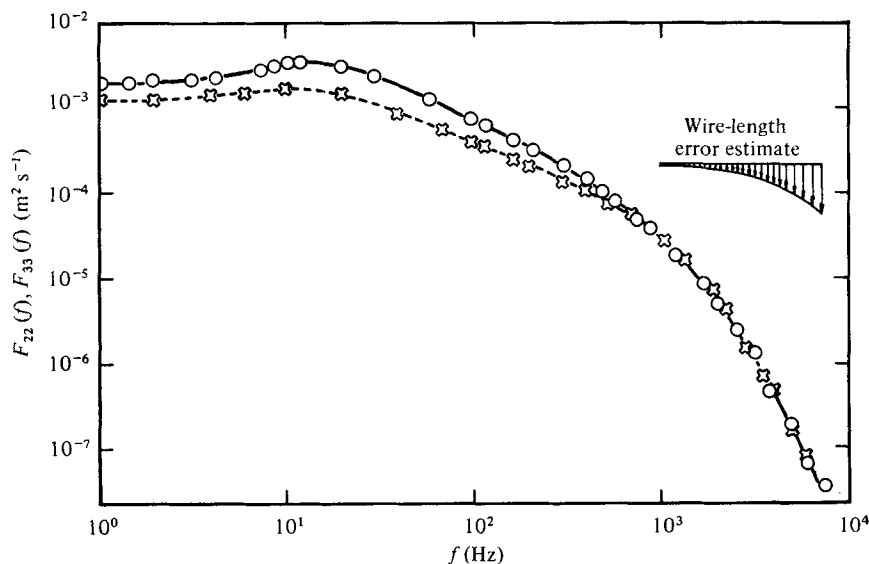
FIGURE 15. One-dimensional spectra of the transverse turbulent velocities.
$\odot$, $F_{22}(f)$; $\bigcirc$, $F_{33}(f)$.
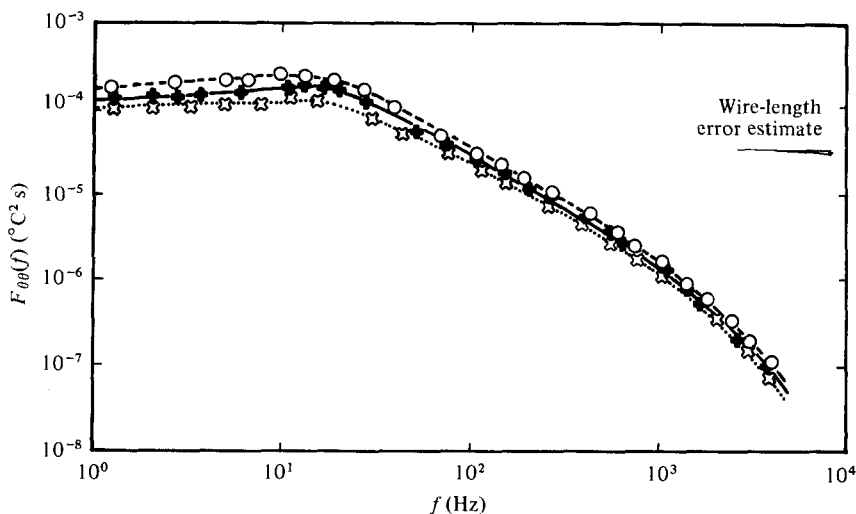
FIGURE 16. One-dimensional temperature spectra.
Ω, $x_1/h = 7\cdot5$; $\blacklozenge$, $x_1/h = 9\cdot5$; $\bigcirc$, $x_1/h = 11\cdot0$.
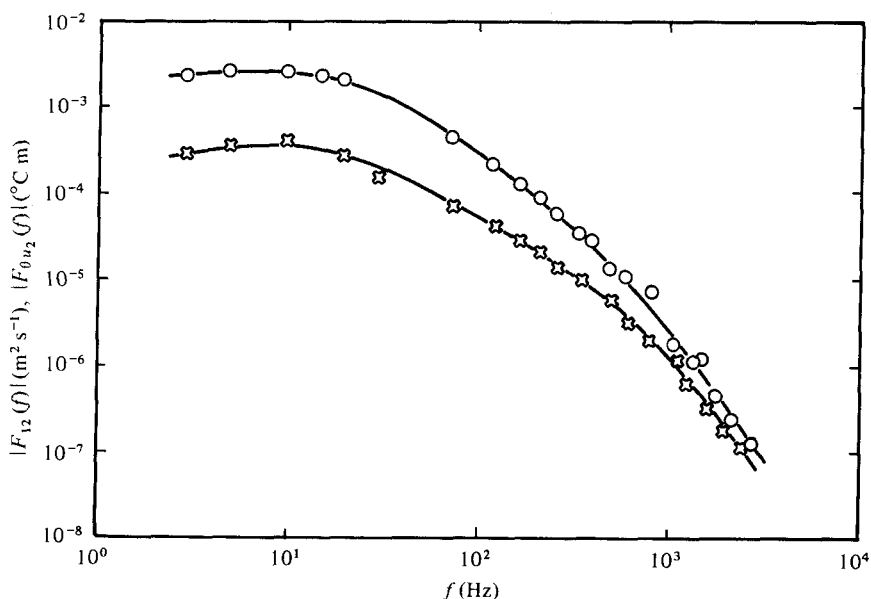
FIGURE 17. One-dimensional cross-spectra of the shear stress and the transverse
heat-transport correlations. $\bigcirc$, $F_{12}(f)$; Ω, $F_{\theta u_2}(f)$.

Reynolds number. The largest relative increase is at the low-frequency region and is
consistent with the downstream increase of the integral length scales. All three spectra
increase slowly with increasing frequency up to about 15 Hz. A near power law region
occurs between roughly 50 Hz and 1 kHz, with a faster decrease starting at $f \approx 1$ kHz,
corresponding to the viscous region; this drop-off is faster than the one due to possible
wire-length errors.

$$L_{11,1} = 57 \text{ mm}, \qquad \lambda_{11} = 5 \cdot 8 \text{ mm}$$

$$L_{11,2}/L_{11,1} = 0 \cdot 33 \qquad L_{\theta\theta,1}/L_{11,1} = 0 \cdot 76$$
$$L_{11,3}/L_{11,1} = 0 \cdot 25 \qquad L_{\theta\theta,2}/L_{11,1} = 0 \cdot 36$$
$$L_{22,1}/L_{11,1} = 0 \cdot 23 \qquad L_{\theta\theta,3}/L_{11,1} = 0 \cdot 31$$
$$L_{33,1}/L_{11,1} = 0 \cdot 34$$
$$L_{12,1}/L_{11,1} = 0 \cdot 90 \qquad L_{\theta u_2,1}/L_{11,1} = 0 \cdot 60$$
$$L_{12,2}/L_{11,1} = 0 \cdot 40\dagger \qquad L_{\theta u_2,2}/L_{11,1} = 0 \cdot 53$$
$$L_{12,3}/L_{11,1} = 0 \cdot 10\dagger \qquad L_{\theta u_2,3}/L_{11,1} = 0 \cdot 24$$
$$\lambda_{12}/\lambda_{11} = 0 \cdot 67 \qquad \lambda_{\theta 1}/\lambda_{11} = 0 \cdot 87$$
$$\lambda_{13}/\lambda_{11} = 0 \cdot 68 \qquad \lambda_{\theta 2}/\lambda_{11} = 0 \cdot 64$$
$$\lambda_{21}/\lambda_{11} = 0 \cdot 68 \qquad \lambda_{\theta 3}/\lambda_{11} = 0 \cdot 64$$
$$\lambda_{31}/\lambda_{11} = 0 \cdot 79$$

† From Harris *et al.* (1977).

TABLE 3. Integral length scales and microscales ($x_1/h = 11 \cdot 0$).

Figure 15 shows the one-dimensional frequency spectra of the transverse velocity components u_2 and u_3, at $x_1/h = 11 \cdot 0$. The low-frequency regions of both spectra show a slight increase with increasing frequency, more pronounced in the case of $F_{33}(f)$. At higher frequencies both decrease monotonically, and they are nearly identical for frequencies higher than about 700 Hz.

The one-dimensional temperature spectra at three downstream stations are shown in figure 16. As in the case of $F_{11}(f)$, $F_{\theta\theta}(f)$ increases downstream at all frequencies, corresponding to the increase of $\overline{\theta^2}$.

The main cross-spectra of interest are the shear-stress spectrum $F_{12}(f)$ and the heat-transfer spectrum $F_{\theta u_2}(f)$. Figure 17 shows their magnitude at $x_1/h = 11 \cdot 0$. The co-herency functions (indicating the degree of local isotropy) and further discussion about the spectra will be given in the second paper.

4.6. *Integral length scales and microscales*

The Eulerian integral length scales of the velocity and the temperature fluctuations represent average sizes of the velocity and temperature structures. Ideally, this scale is defined as the integral of the correlation function. In principle, however, a non-infinite random record or field must have zero integral scale (see, for example, the discussion by Comte-Bellot & Corrsin 1971), so some sort of equivalent quantity is normally computed from data. Here we follow the common practices of integrating the corresponding two-point correlation coefficient to its first zero, if it has one, otherwise to a distance or time at which the correlation becomes 'negligible'. Alternatively, the streamwise integral scales can be computed conveniently by extrapolating the corresponding one-dimensional spectra to zero frequency. The integral scales computed from extrapolated spectra should, in principle, be equal to the *infinite* integrals of the corresponding correlation functions; however, in many experimental situations, the two procedures described here have given nearly equal scales.

Table 3 contains integral length scale values computed from correlation functions at $x_1/h = 11 \cdot 0$; all are normalized with respect to $L_{11,1}$. As expected, appreciable departures from the corresponding isotropic relations occur. For example, the ratios $L_{11,2}/L_{11,1}$ and $L_{11,3}/L_{11,1}$ were $0 \cdot 33$ and $0 \cdot 25$, respectively, whereas they would be $0 \cdot 50$ in isotropic turbulence.
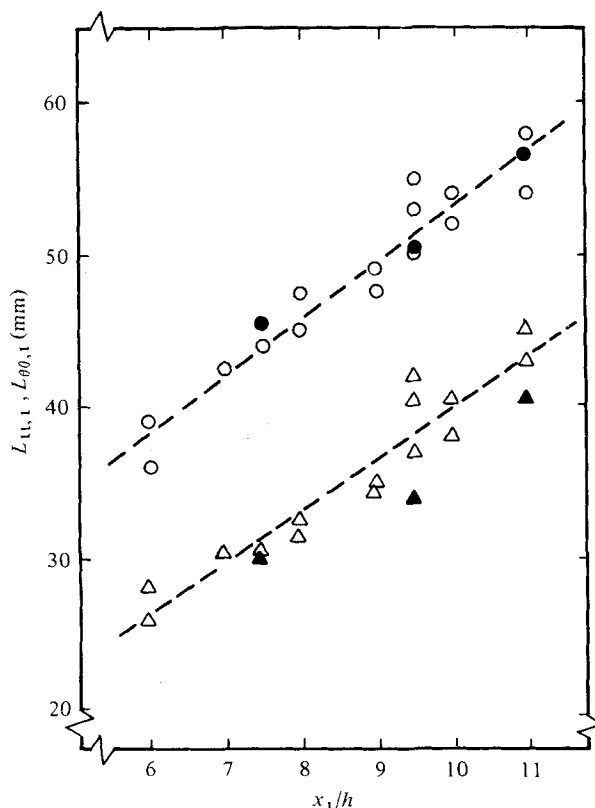
FIGURE 18. Downstream development of the streamwise integral length scales $\bigcirc$, $L_{11,1}$ (from correlations); $\bullet$, $L_{11,1}$ (from spectra); $\triangle$, $L_{\theta\theta,1}$ (from correlations); $\blacktriangle$, $L_{\theta\theta,1}$ (from spectra).

Figure 18 shows the (essentially linear) downstream growth of $L_{11,1}$ and $L_{\theta\theta,1}$ along the tunnel centre-line. The values computed from spectra were not appreciably different from those computed from correlations. Finally, x_2 profiles of these scales showed transverse homogeneity within the (rather large) experimental scatter.

The velocity ('Taylor') microscales and the temperature microscales were measured according to the (isotropic turbulence) definitions (indices not summed):

$$\lambda_{ii} \equiv \left(\frac{\overline{u_i^2}}{\overline{(\partial u_i/\partial x_i)^2}} \right)^{\frac{1}{2}},$$ (12)

$$\lambda_{ij} \equiv \left(\frac{2\overline{u_i^2}}{\overline{(\partial u_i/\partial x_j)^2}} \right)^{\frac{1}{2}}$$ (13)

and

$$\lambda_{\theta i} \equiv \left(\frac{2\overline{\theta^2}}{\overline{(\partial \theta/\partial x_i)^2}} \right)^{\frac{1}{2}}.$$ (14)

Table 3 contains the values at $x_1/h = 11{\cdot}0$. All values have been corrected for electronic noise and for wire length and separation. The transverse microscales are, in general, less reliable than the streamwise ones, since they may contain errors due to differences in the frequency response of the parallel wires; as mentioned earlier,
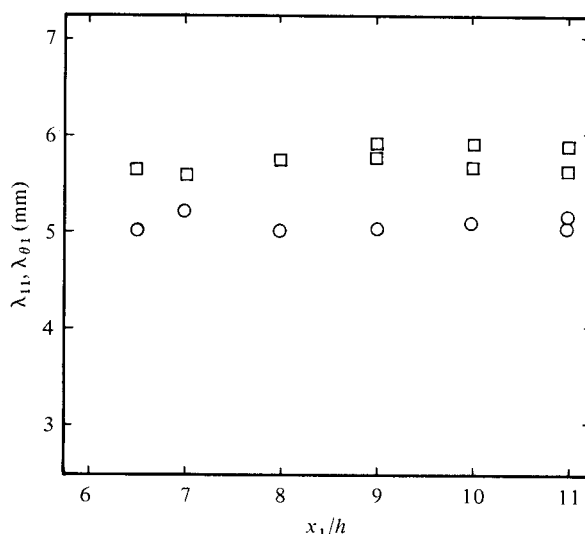
FIGURE 19. Downstream development of the streamwise velocity and temperature microscales. $\square$, λ_{11}; $\bigcirc$, $\lambda_{\theta 1}$.
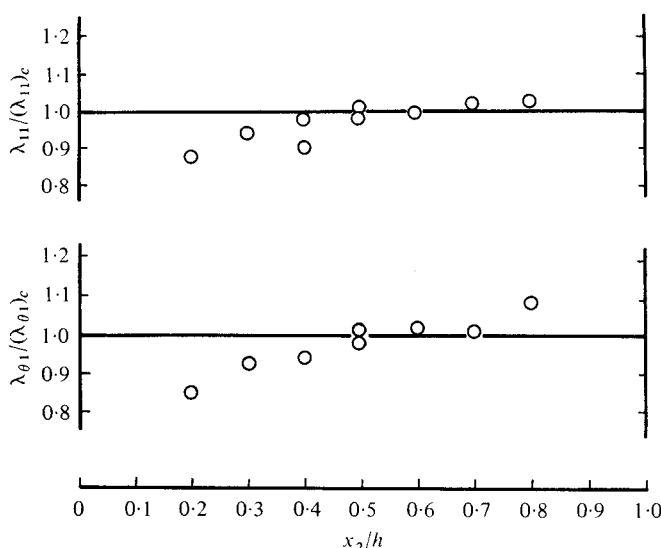
FIGURE 20. Transverse profiles of the streamwise velocity and temperature microscales.

such errors were reduced by matched low-pass filtering of the two signals. Since the energies of different velocity components were unequal, these particular velocity microscales were not expected to be equal, even if the condition of local isotropy were satisfied. In contrast, the unequal values of the three temperature microscales is an explicit demonstration of the departure from the local isotropy of the temperature field.

The downstream development of λ_{11} and $\lambda_{\theta 1}$ on the tunnel centre-line (figure 19) shows approximate constancy of both for $x_1/h > 7\cdot0$. On the other hand, both λ_{11} and $\lambda_{\theta 1}$ increase slightly in the mean shear direction (figure 20). This is consistent with

FIGURE 21. Probability density functions of the turbulent velocities and the temperature
fluctuations. ○, experimental values; – – –, normal distribution.

equations (2) and (6); assuming the isotropic relations $\epsilon \propto u_1^2/\lambda_{11}^2$ and $\chi \propto \theta^2/\lambda_{\theta 1}^2$ approximately valid, λ_{11} and $\lambda_{\theta 1}$ should increase as $\overline{U}_1(x_2)$ increases in the x_2 direction (all other terms were roughly independent of x_2).

4.7. Probabilities

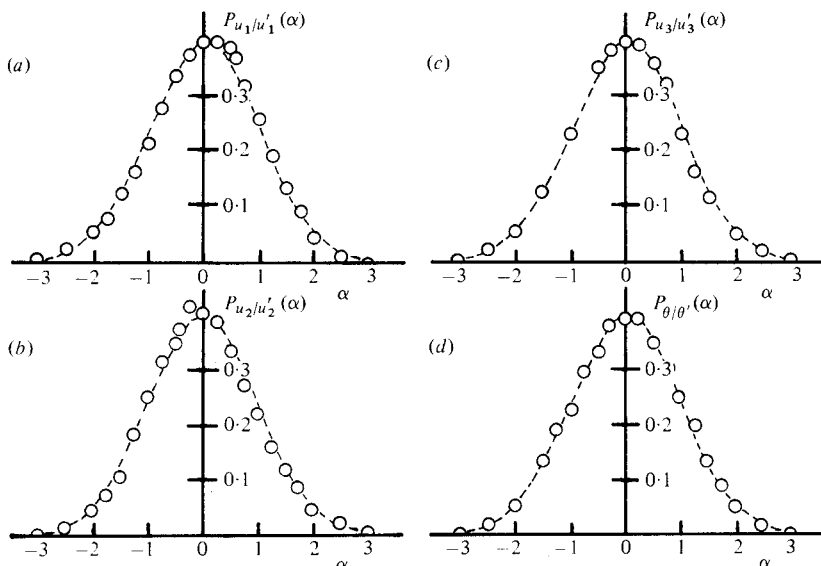Probability and joint probability densities were computed from discrete signal records. Each sample contained about 100000 data points and was about 5 min long.

Measurements of the p.d.f.s (probability density functions) of the three velocity components and the temperature are shown in figure 21; a normal p.d.f. with the same standard deviation is included for reference. The p.d.f.s of u_3 and θ are almost normal, while those of u_1 and u_2 show small departures from normality, consistent with their slight skewnesses.

Equiprobability density functions of the pairs (u_1, u_2), (θ, u_1), and (θ, u_2) are shown in figure 22; the dashed lines are the corresponding contours of jointly normal p.d.f.s with the same correlation coefficients and standard deviations. All pairs appear to be roughly jointly normal, although the skewnesses of u_1 and u_2 imply that the departures from normality are measurable. These joint p.d.f.s can be used to calculate the marginal expectations (by integrating with respect to one variable) and the conditional probabilities (by keeping one variable constant); since all pairs are nearly jointly normal, however, none of these quantities is expected to reveal any additional startling characteristics of the fields.
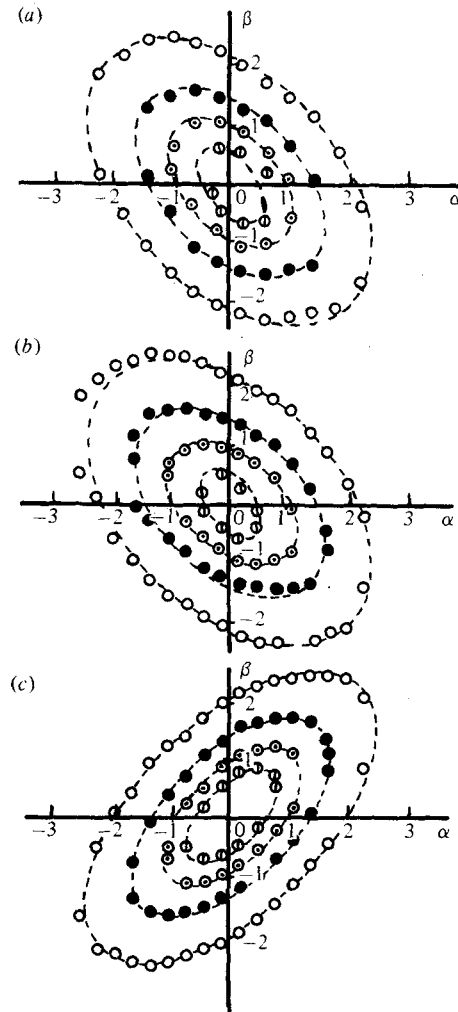
FIGURE 22. Joint probability density functions. (a) $P_{u_1/u_1', u_2/u_2'}(\alpha, \beta)$, (b) $P_{\theta/\theta', u_2/u_2'}(\alpha, \beta)$, and (c) $P_{u_1/u_1', \theta/\theta'}(\alpha, \beta)$. ⊕, $P = 0.15$; ⊙, $P = 0.10$; ●, $P = 0.05$; ○, $P = 0.01$. - - -, jointly normal distribution.

5. Analysis of the experimental results

5.1. Preliminary tests

Several characteristic magnitudes of the velocity and temperature fields on the tunnel centre-line are summarized in table 4. All values correspond to smooth curves fitted to the data by a linear least-squares technique.

A rough check of the buoyancy effect was necessary to ensure that heat was indeed a passive contaminant. A relevant parameter, representing the ratio of the turbulent energy production by density differences to the turbulent energy production by the mean shear, is the 'flux Richardson number',

$$R_f \cong \frac{g}{T} \frac{\overline{\theta u_2}}{\overline{u_1 u_2}\, \partial \overline{U}_1/\partial x_2}, \tag{15}$$

where g is the gravitational acceleration (≈ 9.8 m s^{-2}).

Quantity	$x_1/h = 7\cdot 5$	$x_1/h = 9\cdot 5$	$x_1/h = 11\cdot 0$	Units
$\overline{U}_c$	12·4	12·4	12·4	m s^{-1}
$d\overline{U}_1/dx_2$	46·8	46·8	46·8	s^{-1}
$\overline{u_1^2}$	0·280	0·380	0·475	m² s^{-2}
$\overline{u_2^2}$	0·100	0·134	0·165	m² s^{-2}
$\overline{u_3^2}$	0·156	0·203	0·248	m² s^{-2}
$\overline{q^2}$	0·536	0·717	0·888	m² s^{-2}
$-\overline{u_1 u_2}/u_1' u_2'$	0·45	0·45	0·45	—
$\Delta\overline{T}_c$	1·5	1·5	1·5	°C
$d\overline{T}/dx_2$	9·5	9·5	9·5	°C m^{-1}
$\overline{\theta^2}$	0·0119	0·0134	0·0156	°C²
$\overline{\theta u_1}/\theta' u_1'$	0·53	0·56	0·59	—
$-\overline{\theta u_2}/\theta' u_2'$	0·42	0·435	0·45	—
$L_{11,1}$	44	51	57	mm
$L_{\theta\theta,1}$	31	38	43·5	mm
λ_{11}	5·8	5·8	5·8	mm
$\lambda_{\theta 1}$	5·1	5·1	5·1	mm
ϵ†	1·94	2·65	3·42	m² s^{-3}
η‡	0·204	0·197	0·177	mm
η_θ§	0·263	0·254	0·228	mm

† Turbulent energy dissipation rate, from equation (2).
‡ Kolmogorov microscale, $\eta \equiv (\nu^3/\epsilon)^{\frac{1}{4}}$.
§ Temperature dissipation microscale, $\eta_\theta \equiv (\gamma^3/\epsilon)^{\frac{1}{4}}$.

TABLE 4. Summary of experimental values.

The present experiment corresponds to stable density stratification ($\partial\overline{T}/\partial x_2 > 0$), so that a positive value of R_f is expected. Large positive values of R_f (greater than about 0·2) have a suppressive effect on the vertical turbulent component u_2 and, by nonlinear interactions, on the turbulence as a whole (Tennekes & Lumley 1973). It turns out that $R_f \approx 0\cdot 002 \ll 0\cdot 2$, so buoyancy had a negligible effect on the velocity field.

A related parameter, representing the squared ratio of the time scales associated with production by buoyancy and production by mean shear, is the 'gradient Richardson number'

$$R_g \equiv \frac{g}{T}\frac{\partial\overline{T}/\partial x_2}{(\partial\overline{U}_1/\partial x_2)^2}. \tag{16}$$

Here, $R_g \approx 0\cdot 002 \ll 1$, another confirmation of the negligibility of buoyancy effects.

The inertial effect of temperature-induced density differences on an accelerating flow can be roughly tested with the use of relations (15) and (16) after replacing g by the r.m.s. fluid particle acceleration

$$\alpha \equiv \overline{\left(\frac{\partial\mathscr{V}}{\partial t}\right)^2}^{\frac{1}{2}} = \left(\frac{\overline{\mathscr{V'}^2}}{2\tau^2}\right)^{\frac{1}{2}}. \tag{17}$$

$\mathscr{V}$ is the Lagrangian velocity, τ is the Lagrangian time microscale. For rough calculations, $\overline{\mathscr{V'}^2} \approx \overline{u_1^2}$ and $\tau \approx 5\lambda_{11}/u_1'$ (Shlien & Corrsin 1974), so that $\alpha \approx 10$ m s^{-2}. Thus, the inertial disturbances caused by heating are also negligible away from the heating rods.

Quantity examined N	Measures of downstream inhomogeneity $\dfrac{L_{11,1}}{|N|}\left|\dfrac{\partial N}{\partial x_1}\right|$	Measures of non-stationarity in a frame conveted with the centre-line speed		
		$\dfrac{T_1}{|N|}\left|\dfrac{\partial N}{\partial t}\right|$	$\dfrac{T_2}{|N|}\left|\dfrac{\partial N}{\partial t}\right|$	$\dfrac{T_3}{|N|}\left|\dfrac{\partial N}{\partial t}\right|$
$L_{11,1}$	0·012	0·17	0·23	0·059
λ_{11}	< 0·01	< 0·01	< 0·01	< 0·01
$\overline{q^2}$	0·025	0·35	0·46	0·12
$\overline{u_1 u_2}/u_1' u_2'$	< 0·001	< 0·01	< 0·01	< 0·01
$L_{\theta,1}$	0·015	0·21	0·28	0·072
$\lambda_{\theta 1}$	< 0·01	< 0·01	< 0·01	< 0·01
$\overline{\theta^2}$	0·02	0·28	0·38	0·10
$\overline{\theta u_1}/\theta' u_1'$	0·005	0·07	0·09	0·02
$\overline{\theta u_2}/\theta' u_2'$	0·004	0·05	0·07	0·02

TABLE 5. Measures of downstream inhomogeneity and of non-stationarity in a convected frame $(x_1/h \approx 11\cdot0)$.

The analysis of §2 has shown that, in principle, neither the velocity, nor the temperature fields can be exactly homogeneous. Therefore, it is relevant to look at departures from homogeneity.

Data in §4 show that deviations of the mean square velocity and temperature fluctuations and of the one-point covariances in the central core of the tunnel (extending transversely over several integral length scales) did not exceed 5 % of the corresponding centre-line values. Larger deviations (about 10 %) occurred for the integral length scales $L_{11,1}$ and $L_{\theta\theta,1}$, attributable to large experimental scatter. The only systematic deviations from transverse homogeneity were exhibited by the microscales λ_{11} and $\lambda_{\theta 1}$. Both increased slightly upwards, with maximum deviations in the central core of the tunnel about 8 %.

A general criterion for the downstream spatial near-homogeneity of the statistical quantity N is (see, for example, Champagne *et al.* 1970)

$$\frac{L}{|N|}\left|\frac{\partial N}{\partial x_1}\right| \ll 1, \tag{18}$$

where L is a maximum distance of measurable correlations, taken for convenience to be $L_{11,1}$. The above criterion for characteristic magnitudes of velocity and temperature fields is summarized in the first column of table 5; the values are rough averages over the wind-tunnel final test section $(9\cdot0 < x_1/h < 11\cdot0)$. In these cases, equation (18) is well satisfied.

The temporal evolution of a homogeneous shear flow should be independent of the local mean convection speed, and it is best examined in a frame convected with such a mean speed (in the present case, the centre-line mean speed $\overline{U}_c$). A relation of the form

$$\frac{T}{|N|}\left|\frac{\partial N}{\partial t}\right| \ll 1, \tag{19}$$

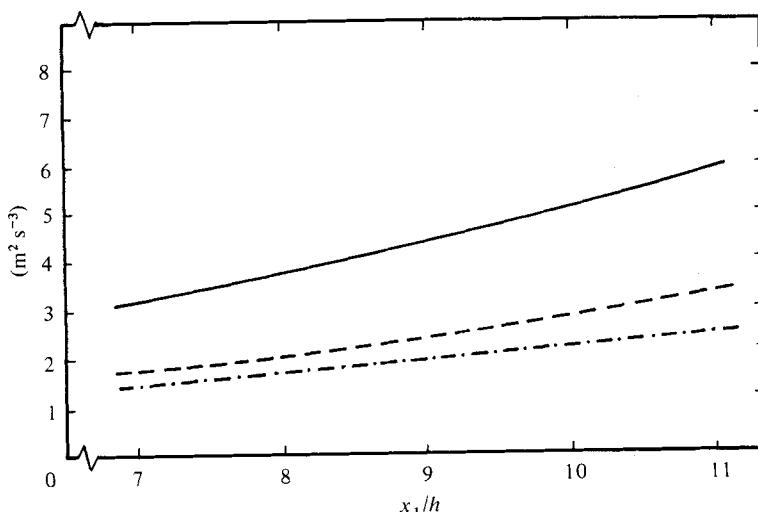where T is a characteristic time in the convected frame, is a test of the near-stationarity

FIGURE 23. Turbulent kinetic energy balance. ———, $-\overline{u_1 u_2}\,d\overline{U}_1/dx_2$; —·—, $\overline{U}_1 d(\tfrac{1}{2}\overline{q^2})/dx_1$; – – –, ϵ from the difference of the other two terms.

of any turbulent characteristic magnitude N. Using Taylor's 'frozen flow' approximation, equation (19) can be written as

$$\frac{T\overline{U}}{|N|}\left|\frac{\partial N}{\partial x_1}\right| \ll 1. \tag{20}$$

A natural characteristic time in the convected frame is

$$T_1 \equiv \int_0^\infty R_{11}(\overline{U}_c\tau,0,0;\tau)\,d\tau \approx 0\cdot061\ \text{s}$$

(Harris *et al.* 1977). A simple kinematic time of the most energetic eddies (the 'eddy turnover time') is

$$T_2 \equiv \frac{L_{11,1}}{u_1'} \approx 0\cdot081\ \text{s},$$

roughly the same as T_1. Another characteristic time, that of the mean strain rate, is

$$T_3 \equiv \left(\frac{\partial \overline{U}_1}{\partial x_2}\right)^{-1} \approx 0\cdot021\ \text{s},$$

significantly smaller than the other two.

Tests of the moving-frame non-stationarity of the flow are provided in the last three columns of table 5. Equation (19) is well satisfied in most cases and fairly well in the others. $L_{11,1}$, $L_{\theta\theta,1}$, and (especially) $\overline{q^2}$ and $\overline{\theta^2}$ appear to depart appreciably from stationarity.

5.2. *The governing equations*

The balance of the mean turbulent kinetic energy is approximately described by equation (2). The convection and production terms are directly measurable with typical error bounds $\pm 5\%$, while all omitted terms (estimated or measured) were
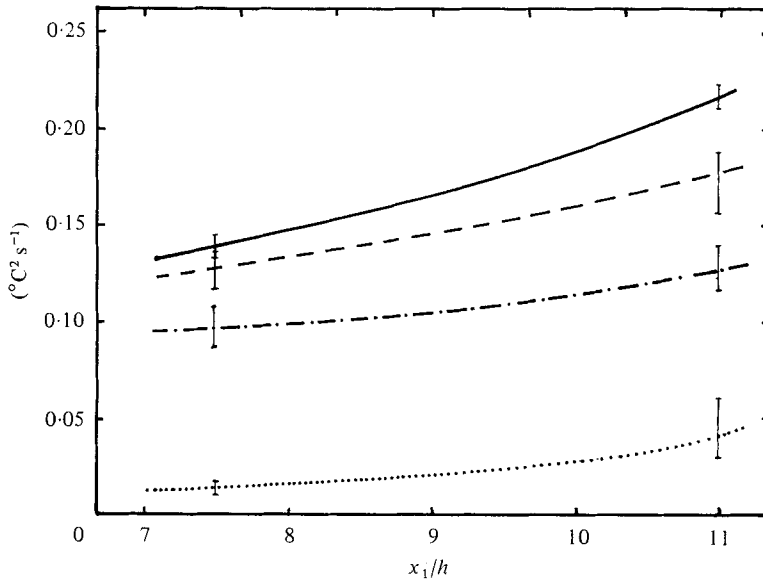
FIGURE 24. Temperature fluctuation balance. ——, $-\overline{\theta u_2} d\overline{T}/dx_2$; $\cdots\cdots$, $\frac{1}{2}\overline{U}_1 d\overline{\theta^2}/dx_1$; $---$, χ from the difference of the other two terms; $-\cdot-$, χ from the measured mean square temperature derivatives. The vertical lines represent estimated error bounds.

less than 1 % of the production. The dissipation rate can be conveniently estimated as the imbalance of the other two terms in equation (2), since its direct measurement is subject to larger experimental inaccuracies. Figure 23 shows that the three terms in equation (2) increase in magnitude downstream; however, their ratios remain roughly constant, with transport being about 45 % of the production by the mean shear. The sum of five independently measured mean-squared velocity derivatives differs by only 8 % from its locally isotropic estimate based on the estimated dissipation rate.

The balance of $\overline{\theta^2}$ is approximately described by equation (5) or, after omission of negligible terms (measured to be less than 1 % of the production terms), by equation (6). Figure 24 shows the downstream development of the three terms in equation (6); estimated error bounds are included. The production term was measured directly. The transport term (especially at $10\cdot0 < x_1/h$) was sensitive to the choice of the smooth curve fitted to the $\overline{\theta^2}$ data. A parabola was clearly inadequate for the accurate estimation of $d\overline{\theta^2}/dx_1$; a cubic polynomial was the simplest curve to represent the data fairly well in the range $6\cdot0 < x_1/h < 11\cdot0$; a fourth-order polynomial gave a better fit but introduced inflection points attributable to scatter rather than the physical process. The thermal 'dissipation' rate χ could be estimated either as the imbalance of the other two terms or directly from the measured mean-squared temperature derivatives (see measurement of microscales, §4.6). The two procedures gave values differing by about 30 %. Such a difference remains inexplicable, since it is somewhat larger than the estimated experimental errors; it seems likely that the actual χ lies between its two estimates.

The simplified balance equations for the temperature–velocity covariances, equations (7) and (8), contain the pressure covariance terms which cannot be measured

accurately enough with instruments available at present. The 'dissipation' terms (last terms on the right-hand side of both equations) can be measured with present techniques, but the accuracy would be limited. The directly measured terms at $x_1/h = 11 \cdot 0$ were as follows:

$$\overline{U}_1 \frac{d\overline{\theta u_1}}{dx_1} \approx 0 \cdot 30 \; °\text{C m s}^{-2}, \quad -\overline{\theta u_2}\frac{d\overline{U}_1}{dx_2} \approx 1 \cdot 06 \; °\text{C m s}^{-2},$$

$$-\overline{u_1 u_2}\frac{d\overline{T}}{dx_2} \approx 1 \cdot 19 \; °\text{C m s}^{-2}, \quad \overline{U}_1 \frac{d\overline{\theta u_2}}{dx_1} \approx -0 \cdot 13 \; °\text{C m s}^{-2},$$

$$-\overline{u_2^2}\frac{d\overline{T}}{dx_2} \approx -1 \cdot 56 \; °\text{C m s}^{-2}, \quad (\gamma+\nu)\overline{\frac{\partial u_2}{\partial x_1}\frac{\partial \theta}{\partial x_1}} \approx -0 \cdot 03 \; °\text{C m s}^{-2},$$

$$\left|\frac{d\overline{\theta u_1^2}}{dx_1}\right|, \left|\frac{d\overline{\theta u_1 u_2}}{dx_1}\right| < 0 \cdot 01 \; °\text{C m s}^{-2}.$$

5.3. *Calculation of characteristic transport parameters*

The mean strain rate tensor $\{\partial \overline{U}_i/\partial x_k + \partial \overline{U}_k/\partial x_i\}$ has only two non-zero components, both equal to $d\overline{U}_1/dx_2$. As in any parallel mean flow, two of its principal axes form $\pm 45°$ angles with x_1; the third one coincides with x_3.

The mean turbulent Reynolds-stress tensor $\{-\overline{u_i u_k}\}$ takes the form

$$\{-\overline{u_i u_k}\} = \left\{ \begin{matrix} \overline{u_1^2} & -\overline{u_1 u_2} & 0 \\ -\overline{u_1 u_2} & \overline{u_2^2} & 0 \\ 0 & 0 & \overline{u_3^2} \end{matrix} \right\}. \tag{21}$$

Following Corrsin (1957) we look at the three principal stresses,

$$\left. \begin{aligned} -\sigma_a, -\sigma_b &= \frac{\overline{u_1^2}+\overline{u_2^2}}{2} \pm \left[\left(\frac{\overline{u_1^2}-\overline{u_2^2}}{2}\right)^2 + (\overline{u_1 u_2})^2 \right]^{\frac{1}{2}}, \\ -\sigma_c &= -\overline{u_3^2}. \end{aligned} \right\} \tag{22}$$

The directions of the first two principal axes are, respectively,

$$\alpha_a, \alpha_b = \tfrac{1}{2}\arctan\left(\frac{\pm 2\overline{u_1 u_2}}{\overline{u_1^2}-\overline{u_2^2}}\right). \tag{23}$$

The ratios σ_a/σ_b and σ_a/σ_c as well as the angle α_a were nearly constant within the test volume (table 6) with values close to those reported by Harris *et al.* (1977) and similar to those in turbulent boundary layers and channels (Corrsin 1957).

The turbulent momentum diffusivity tensor is, in general, of fourth order (see, for instance, Hinze 1975). However, its only distinct measurable component is the traditional (scalar) 'turbulent viscosity' or 'eddy viscosity',

$$\nu_T \equiv \frac{-\overline{u_1 u_2}}{d\overline{U}_1/dx_2}. \tag{24}$$

The thermal turbulent diffusivity tensor D_{ij} (Batchelor 1949) in the present case has two distinct measurable components

$$D_{12} \equiv \frac{-\overline{\theta u_1}}{d\overline{T}/dx_2}, \quad D_{22} \equiv \frac{-\overline{\theta u_2}}{d\overline{T}/dx_2}. \tag{25}, (26)$$

The latter is the traditional 'turbulent thermal diffusivity' or 'eddy diffusivity', γ_T.

x_1/h ...	7·5	9·5	11·0
σ_a/σ_b	4·2	4·3	4·3
σ_a/σ_c	2·0	2·1	2·1
$\alpha_a[°]$	20	20	20
ν_T/ν	107	145	179
γ_T/γ	72	93	114
σ_T	1·06	1·11	1·12
D_{12}/D_{22}	−2·1	−2·2	−2·2
B	1·36	1·48	1·53
R_{λ_g}	128	147	160
$R_{\lambda_{11}}$	205	238	266
$\dfrac{\lambda_g}{L_g}R_{\lambda_g}$	36·9	36·0	34·4
P_{λ_θ}†	69 (79)	77 (91)	86 (102)
$P_{\lambda_{\theta_1}}$	129	150	167
$\dfrac{L_\theta}{\lambda_\theta}P_{\lambda_\theta}$†	12·2 (16·0)	10·7 (15·0)	10·5 (14·6)
$\tau_u[s]$	0·27	0·27	0·26
$\tau_\theta[s]$†	0·093 (0·12)	0·087 (0·12)	0·088 (0·12)
τ_θ/τ_u†	0·34 (0·44)	0·32 (0·44)	0·34 (0·46)

† The first values correspond to χ estimated from the imbalance of transport and production in equation (6); the values in parentheses correspond to χ computed from the sum of the mean-squared temperature derivatives.

TABLE 6. Characteristic transport parameters.

The ratios ν_T/ν and γ_T/γ increase rapidly downstream (table 6), demonstrating the increasing importance of turbulent diffusion with respect to molecular diffusion; nevertheless, the turbulent Prandtl number σ_T ($\equiv \nu_T/\gamma_T$) and the ratio of thermal diffusivities D_{12}/D_{22} are nearly constant in the test volume.

The ratio

$$B \equiv \frac{q'}{d\overline{U}_1/dx_2}\bigg/\frac{\theta'}{d\overline{T}/dx_2} \tag{27}$$

represents the relative strength of turbulent velocity versus temperature fluctuations. Here, B was slightly increasing downstream to a value near 1·5 (notice that Fulachier & Dumas (1976) have shown that $B \approx 1·5$ across a turbulent boundary layer).

The turbulent Reynolds number R_{λ_g} and Péclet number P_{λ_θ} are dimensionless measures of the local 'strength' of turbulence compared to the molecular actions. The isotropic definitions

$$R_{\lambda_g} \equiv \frac{u\lambda_g}{\nu}, \quad P_{\lambda_\theta} \equiv \frac{u\lambda_\theta}{\gamma} \tag{28, 29}$$

are ambiguous in non-isotropic turbulence, where the mean-squared velocity fluctuations and the microscales are directionally dependent. An average root-mean-square velocity fluctuation can be defined as

$$u \equiv (\tfrac{1}{3}\overline{q^2})^{\frac{1}{2}}. \tag{30}$$

Although local isotropy does not apply to this flow (see second paper), some average microscales λ_g and λ_θ can be computed from the turbulent energy and thermal fluctuation dissipation rates with the use of the isotropic relations

$$\epsilon \equiv 15\nu \frac{\overline{u^2}}{\lambda_g^2}, \tag{31}$$

and

$$\chi \equiv 6\gamma \frac{\overline{\theta^2}}{\lambda_\theta^2}. \tag{32}$$

Alternatively, the streamwise turbulent Reynolds and Péclet numbers (often used in inhomogeneous turbulence studies) can be defined as

$$R_{\lambda_{11}} \equiv \frac{u_1' \lambda_{11}}{\nu}, \quad P_{\lambda_{\theta 1}} \equiv \frac{u_1' \lambda_{\theta 1}}{\gamma}. \tag{33}, (34)$$

Table 6 contains the values of the turbulent Reynolds and Péclet numbers in three downstream stations. A monotonic increase of all numbers is observed, corresponding mainly to the downstream increase of u (or u_1').

The dimensionless products $(\lambda_g/L_g)\,R_{\lambda_g}$ and $(\lambda_\theta/L_\theta)\,P_{\lambda_\theta}$ should be constants according to the dynamic similarity theories (von Kármán & Howarth 1938; Corrsin 1951), and in fact have shown only small variation during the decay of grid-generated turbulence (Comte-Bellot & Corrsin 1971; Sreenivasan *et al.* 1980). In order to compensate partially for the directional dependence of the integral length scales, it was decided to use the following 'average values':

$$L_g \equiv \tfrac{1}{3}(\tfrac{1}{2}L_{11,1} + L_{11,2} + L_{11,3}) \approx 0{\cdot}36 L_{11,1} \tag{35}$$

and

$$L_\theta \equiv \tfrac{1}{3}(L_{\theta\theta,1} + L_{\theta\theta,2} + L_{\theta\theta,3}) \approx 0{\cdot}63 L_{\theta\theta,1}. \tag{36}$$

As shown in table 6, $(\lambda_g/L_g)\,R_{\lambda_g}$ and $(\lambda_\theta/L_\theta)\,P_{\lambda_\theta}$ decrease downstream but slowly enough to be considered essentially constants. $(\lambda_g/L_g)\,R_{\lambda_g}$ is somewhat larger and $(\lambda_\theta/L_\theta)\,P_{\lambda_\theta}$ is somewhat smaller than the corresponding values in grid turbulence.

An intrinsic measure of turbulent activity is the relative 'life-time' of the energy-containing eddies, $\tau_u \equiv \overline{q^2}/\epsilon$. Similarly, the time-scale $\tau_\theta \equiv \overline{\theta^2}/\chi$ is a measure of the relative 'life-time' of temperature fluctuations. As shown in table 6, both τ_u and τ_θ are essentially constant.

6. Further discussion

6.1. *The downstream evolution of the velocity and the temperature fluctuation fields*

As shown earlier, the mean velocity gradient as well as the mean temperature gradient remained practically constant within the test volume

$$(7{\cdot}5 \leqslant x_1/h \leqslant 11{\cdot}0, \quad 0{\cdot}2 \leqslant x_2/h \leqslant 0{\cdot}8);$$

furthermore, both the velocity and the temperature fluctuation fields retained a reasonable degree of transverse homogeneity within the same volume. Consequently, the only relevant independent variable was the downstream distance x_1 from the shear-flow generator. The wind-tunnel height, h, used for normalizing x_1 is, of course, irrelevant in the central core of the tunnel because there are no boundary effects.
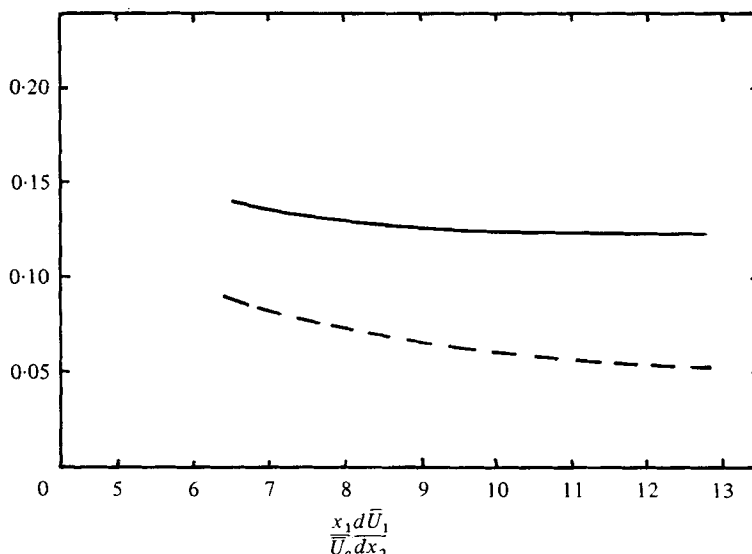
FIGURE 25. Downstream evolution of the normalized turbulent kinetic energy and temperature
fluctuations. ——, $\overline{q^2}/(L_{11,1}d\overline{U}_1/dx_2)^2$; – – –, $\overline{\theta^2}/(L_{11,1}d\overline{T}/dx_2)^2$.

The width w of the shear-flow-generating channels is more meaningful as an initial
length scale. Indeed, the integral length scales are the same order as w over the test
region. In any case, away from the origin there is no externally imposed length or
velocity scale (the convection velocity $\overline{U}_c$ should be irrelevant because the field should
be independent of a Galilean transformation) and the flow develops presumably under
the influence of the mean shear only. The inverse of the mean shear $(d\overline{U}_1/dx_2)^{-1}$ can be
considered as an imposed (constant) time scale.

The dimensionless evolution time (otherwise interpreted as a 'total strain')

$$\tau \equiv \frac{x_1}{\overline{U}_c}\frac{dU_1}{dx_2}$$

was used by Harris *et al.* in comparisons of the high-shear (Harris *et al.*) and the low-
shear (Champagne *et al.*) cases. Such a parameter should be adequate for describing the
development of the present flow (or flows generated with similar devices) but in general
it cannot be used for comparisons with more complex, inhomogeneous shear flows.

The present section is a comparative study of the downstream development of the
velocity and temperature fluctuation fields, both of which increase monotonically in
mean-squared value. Evidently, for each quantity the production exceeds the 'dissi-
pation'. A downstream increase of the integral length scales was also observed. It is
of interest to see whether the mean-squared velocity and temperature fluctuations
can be normalized to constant, asymptotic values. A natural way of normalizing $\overline{q^2}$
and $\overline{\theta^2}$ appears to be

$$\frac{\overline{q^2}}{(L_{11,1}d\overline{U}_1/dx_2)^2} \tag{37}$$

(Harris *et al.*) and

$$\frac{\overline{\theta^2}}{(L_{11,1}d\overline{T}/dx_2)^2}. \tag{38}$$

Expressions (37) and (38) have been plotted versus τ in figure 25. It is clear that the dimensionless turbulent kinetic energy is nearly constant in the downstream region ($9 < \tau < 12\cdot5$), while the dimensionless thermal energy is still decreasing, suggesting that the velocity field has reached an asymptotic state, while the temperature field has not. Nevertheless, the slope of expression (38) is decreasing at $\tau = 12\cdot5$, so an asymptotic state for the temperature field might be reached at slightly higher values of τ. Another indication that the velocity fluctuation field has reached an asymptotic state while that of temperature had not was the fact that the shear-stress correlation $\overline{u_1 u_2}/u_1' u_2'$ was nearly constant but the heat transport correlations $\overline{\theta u_1}/\theta' u_1'$ and $-\overline{\theta u_2}/\theta' u_2'$ were still increasing slowly.

On the other hand, some results suggest that both fields evolved in comparable ways. The velocity and the temperature integral scales presented nearly equal rates of downstream increase. Both the velocity and the temperature microscales were nearly constant in the test volume. Although the turbulent viscosity ν_T and the turbulent diffusivity γ_T were monotonically increasing downstream, their ratio (the turbulent Prandtl number σ_T) was practically constant. Finally, both $(\lambda_g/L_g) R_{\lambda_g}$ and $(\lambda_\theta/L_\theta) P_{\lambda_\theta}$ as well as both τ_u and τ_θ showed only small variations in the test volume.

In conclusion, it appears that most of the velocity data reported here (the ones at $7\cdot5 \leqslant x_1/h \leqslant 11\cdot0$) correspond to an asymptotically developed, varying flow field,† but only measurements near the last station ($x_1/h \approx 11\cdot0$) correspond to a nearly asymptotic temperature fluctuation field.

6.2. *Correlations of the velocity and temperature*

Analogies and differences between the turbulence structure of the homogeneous shear flow and that of inhomogeneous turbulence can be revealed by comparisons of the corresponding one-point and two-point correlation coefficients. However, such comparisons are only a secondary aim of the present report and they will be limited. As typical examples of inhomogeneous turbulence we shall consider the fully turbulent regions of a boundary layer and of pipe flow. Considerable similarities between the above flows and homogeneous sheared turbulence are expected, since the relative magnitudes and the orientations of the principal Reynolds stresses were roughly the same (Champagne *et al.* 1970; Harris *et al.* 1977).

A comparative study of the three turbulent shear flows is given in table 7. In the latter two cases, of course, the reported quantities exhibit some transverse variation; this is relatively slow, however, and the values in table 7 are typical. Evidently the one-point correlation coefficients have comparable magnitudes in the three flows. The differences in signs are merely a reflexion of the differences in the direction of $\partial \overline{T}/\partial x_2$ with respect to $\partial \overline{U}_1/\partial x_2$.

The only components of the two-point space correlation coefficient tensor

$$R_{ij}(r_1, r_2, r_3; 0)$$

reported here were $R_{11}(r_i)$ and $R_{ii}(r_1)$, $i = 1, 2, 3$, not summed. The simplified notation

---

† In an unpublished report, Sreenivasan (1979) concluded that, based on the development of 'structural parameters' introduced by Townsend (1954), an asymptotic stage of the velocity field was reached at $x_1/h \approx 5\cdot0$.

Flow	R_λ	$\dfrac{\overline{u_1 u_2}}{u_1' u_2'}$	$\dfrac{\overline{\theta u_1}}{\theta' u_1'}$	$\dfrac{\overline{\theta u_2}}{\theta' u_2'}$	$\dfrac{D_{12}}{D_{22}}$	σ_t
Homogeneous shear flow ($x_1/h = 11 \cdot 0$)	160	$-0 \cdot 45$	$0 \cdot 59$	$-0 \cdot 45$	$-2 \cdot 2$	$1 \cdot 1$
Turbulent boundary layer† ($x_2/\delta_M = 1$; δ_M is the momentum thickness)	90–120	$-0 \cdot 42$	$-0 \cdot 66$	$0 \cdot 50$	$-2 \cdot 4$	$1 \cdot 1$
Turbulent pipe flow ($r/d = 0 \cdot 25$; d is the diameter)	80–300	$-0 \cdot 47‡$	$-0 \cdot 63§$	$0 \cdot 43\|$	$-2 \cdot 1$	$1 \cdot 2¶$

† Johnson (1957, 1959). ‡ Laufer (1954). § Bremhorst & Bullock (1970).
‖ Bourke & Pulling (1970). ¶ Schwarz & Hoelscher (1956).

TABLE 7. A comparative study of three turbulent shear flows.

$R(r_i)$ implies that the only non-zero separation of the probes was in the x_i direction. It was found that

$$R_{11}(r_1) > R_{11}(r_2) > R_{11}(r_3)$$

(the first inequality is stronger than that in isotropic turbulence where

$$R_{11}(r_2) = R_{11}(r_1) + \tfrac{1}{2} r_1 \, \partial R_{11}(r_1)/\partial r_1$$

with $r_1 = r_2$) and

$$R_{11}(r_1) > R_{33}(r_1) > R_{22}(r_1).$$

The same ordering of the corresponding coefficients was observed in a turbulent boundary layer (Grant 1958) and in channel flow (Comte-Bellot 1961). This is another confirmation of the close structural resemblance between these 'classical' flows and homogeneous shear turbulence.

It was observed that the temperature fluctuations follow u_1 more closely than u_2. The result

$$R_{\theta\theta}(r_1) > R_{\theta\theta}(r_2) > R_{\theta\theta}(r_3)$$

(figure 12) supports the latter statement. In an isotropic temperature field the three correlations are equal.

The heat-transport correlation coefficients (figure 13) were ordered as

$$-R_{\theta u_2}(r_1) \geqslant -R_{\theta u_2}(r_2) > -R_{\theta u_2}(r_3).$$

The same ordering (although with stronger inequalities) was observed for the shear-stress correlation coefficients $R_{12}(r_i)$ (Harris *et al.*, figure 12).

The isocorrelation contours of $R_{\theta\theta}$ and $R_{\theta u_2}$ in the x_1, x_2 plane have a 'tilted oval' asymmetric form due to the action of the mean shear, while those in the x_1, x_3 plane were nearly symmetric. Like shapes were observed for the corresponding isocorrelation contours of R_{11} and R_{12} (Harris *et al.*, figures 10, 11 and 14). The corresponding contours in turbulent boundary-layer and channel flows are of comparable shapes but somewhat distorted by inhomogeneity.

A comparison of the autocorrelations R_{11}, R_{22}, and $R_{\theta\theta}$ in a frame moving with the
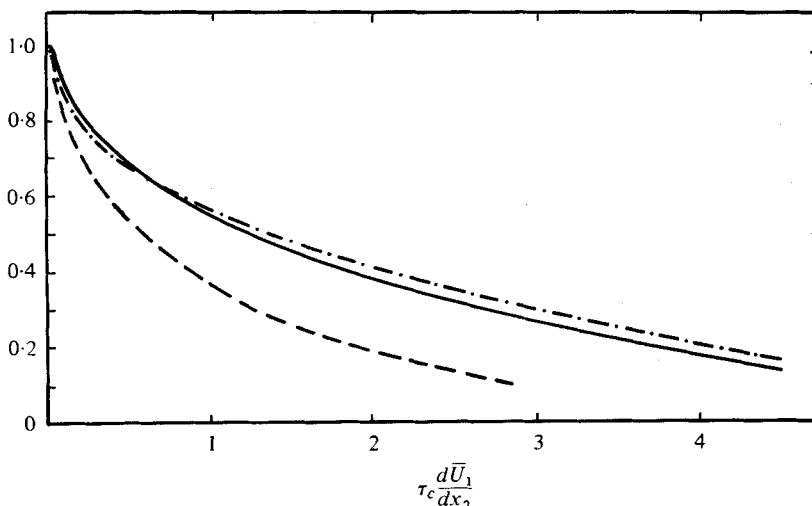
FIGURE 26. Envelopes of the space–time correlations. — · —, $R_{11}(\overline{U}_c\tau_c, 0, 0; \tau_c)$;
– – –, $R_{22}(\overline{U}_c\tau_c, 0, 0; \tau_c)$, from Harris *et al.*; ——, $R_{\theta\theta}(\overline{U}_c\tau_c, 0, 0; \tau_c)$.

mean speed is given in figure 26. $R_{\theta\theta}(\tau_c)$ is nearly equal to $R_{11}(\tau_c)$, while $R_{22}(\tau_c)$ significantly lower than the other two.

6.3. *On the turbulent diffusivity tensor and the turbulent Prandtl number*

The non-zero value of the cross-component D_{12} of the thermal diffusivity tensor D_{ij} sharply dramatizes the inadequacy of all scalar 'eddy diffusivity' theories, which assume in effect that D_{ij} is diagonal. The result $D_{12} \neq 0$ is not novel. Yaglom (1969) showed by qualitative arguments that $D_{12} < 0$ in a turbulent flow with $\partial \overline{U}_1/\partial x_2 > 0$ and $\partial \overline{T}/\partial x_2 < 0$; he also pointed out that in general $D_{12} \neq D_{21}$, namely that the turbulent diffusivity tensor should not be expected to be symmetric (the latter argument was presented earlier by Gee & Davis (1964)). The asymmetry of D_{ij} in a shear flow with constant $\partial \overline{T}/\partial x_1$ and $\partial \overline{T}/\partial x_2$ was proved by Corrsin (1973), who also derived explicit expressions for the components of D_{ij}.

In view of the earlier observation that $|\overline{\theta u_1}/\theta' u_1'| > |\overline{\theta u_2}/\theta' u_2'|$, it should not be surprising that $|D_{12}| > |D_{22}|$. A mildly surprising fact is the near equality of the values of the ratio D_{12}/D_{22} in the three turbulent flows examined in the previous section. They were $-2{\cdot}2$ in the homogeneous shear flow, $-2{\cdot}4$ in the turbulent boundary layer $(x_2/\delta_M = 1{\cdot}0)$ and $-2{\cdot}1$ in the fully developed pipe flow $(x_2/d = 0{\cdot}25)$.

The possible ('Reynolds') analogy between heat transport and momentum transport in nearly parallel turbulent flows is commonly examined in terms of the 'turbulent Prandtl number' σ_T. 'Perfect' analogy corresponds to $\sigma_T = 1$. In the present flow, $\sigma_T \approx 1{\cdot}1$. The corresponding value in the turbulent boundary layer was also about $1{\cdot}1$ and that in the pipe flow was $1{\cdot}2$.

A simple expression for σ_T in exactly homogeneous and stationary turbulence with uniform mean velocity and mean temperature gradients was derived by Corrsin (1952), based on the assumptions of local isotropy and stationarity, and using empirical constants. The result is not applicable to the present experiments because the downstream increase in $\overline{q^2}$ and $\overline{\theta^2}$ here corresponds to non-stationarity in a convected frame.

Deissler (1962) estimated σ_T in homogeneous shear flow with uniform mean temperature gradient by solving the spectral equations of heat transfer after neglecting all terms corresponding to third moments. Although his solution corresponded to 'weak', decaying turbulence, it predicted that, for sufficiently high velocity gradients, the turbulent Prandtl number was approximately 1, and that the two corresponding correlation coefficients were about -0.5.

7. Concluding remarks

The simplest case in a possible series of experiments in 'simple' heated turbulent shear flows, that with uniform mean velocity gradient and mean temperature gradient, was measured in some detail. As in the unheated case, the properties are much like those in channel flows and in the fully turbulent region of boundary layers. However, since the basic parameters of the problem, the mean velocity gradient and the mean temperature gradient, were not varied, it was not possible to examine how their variation would affect various transport and mixing properties, in particular the temperature–velocity correlations, the components of the turbulent diffusivity tensor, and the turbulent Prandtl number.

It would clearly be desirable to study flows with different combinations of mean velocity and mean temperature profiles. The easiest ones experimentally could be produced by retaining the same mean shear and changing the mean temperature gradient. The quantitative effect of such a change on the turbulent transport properties is not *a priori* obvious, even for the case with a mean temperature gradient of magnitude equal but direction opposite to the present one.

Of particular future interest would be the case of much higher heating, when buoyancy effects would become significant. A principal technical problem might be the requirement of a longer distance to achieve an asymptotic, 'moving equilibrium' state.

For the study of additional off-diagonal components of the turbulent diffusivity tensor, a mean temperature gradient which is not parallel to the mean velocity gradient would be in order. This might be achieved with the use of non-uniform wiring of the horizontal heating rods. Such an investigation is currently under way.

More serious modifications of the system would be required to increase the mean velocity profile. Furthermore, although the present mean shear, $46.8\ \mathrm{s^{-1}}$, is not uncommon in other shear flows (in a typical laboratory low-speed turbulent boundary layer studied by Johnson (1957, 1959), one momentum thickness away from the wall the mean shear was $65\ \mathrm{s^{-1}}$), it might be desirable to increase the mean shear, or perhaps preferably the turbulent Reynolds number by one order of magnitude.

REFERENCES

ALEXOPOULOS, C. C. & KEFFER, J. F. 1971 Turbulent wake in a passively stratified field. *Phys. Fluids* **14**, 216.

BATCHELOR, G. K. 1949 The role of big eddies in homogeneous turbulence. *Proc. Roy. Soc. A* **195**, 513.

BOURKE, P. J. & PULLING, D. J. 1970 A turbulent heat flux meter and some measurements of turbulence in air flow through a heated pipe. *Int. J. Heat Mass Transfer* **13**, 1331.

BREMHORST, K. & BULLOCK, K. J. 1970 Spectral measurements of temperature and longitudinal velocity fluctuations in fully developed pipe flow. *Int. J. Heat Mass Transfer* **13**, 1313.

BURGERS, J. M. & MITCHNER, M. 1953 On homogeneous non-isotropic turbulence connected with a mean motion having a constant velocity gradient. *Konik. Ned. Akad. v. Wet. B* **15**, 228; Part II, 383.

CHAMPAGNE, F. H., HARRIS, V. G. & CORRSIN, S. 1970 Experiments on nearly homogeneous turbulent shear flow. *J. Fluid Mech.* **41**, 81.

COMTE-BELLOT, G. 1961 Corrélations spatiales doubles des fluctuations de vitesse dans un tunnel bidimensionnel à parois parallèles. *C.R. Acad. Sci. Paris* **253**, 2846.

COMTE-BELLOT, G. & CORRSIN, S. 1971 Simple Eulerian time correlation of full- and narrow-band velocity signals in grid-generated, 'isotropic' turbulence. *J. Fluid Mech.* **48**, 273.

CORRSIN, S. 1950 Hypothesis for the skewness of the probability density of the lateral velocity fluctuations in turbulent shear flow. *J. Aero. Sci.* **17**, 396.

CORRSIN, S. 1951 The decay of isotropic temperature fluctuations in isotropic turbulence. *J. Aero. Sci.* **18**, 417.

CORRSIN, S. 1952 Heat transfer in isotropic turbulence. *J. Appl. Phys.* **23**, 113.

CORRSIN, S. 1953 Remarks on turbulent heat transfer. *Proc. Iowa Thermo. Symp.* 5, *State Univ. of Iowa, Iowa City.*

CORRSIN, S. 1957 Some current problems in turbulent shear flows. *Proc. 1st Naval Hydr. Symp.*, Nat. Acad. Sci./Nat. Res. Counc., Washington, DC, publ. no. 515.

CORRSIN, S. 1963 Turbulence: experimental methods. *Handbuch der Physik VIII/2*, 524 (ed. S. Flügge & C. Truesdell). Springer.

CORRSIN, S. 1973 A theoretical estimate of the turbulent diffusivity tensor in homogeneous shear flow (abstract). *Bull. Amer. Phys. Soc.* **18**, 1473.

CRAYA, A. 1958 Contribution à l'analyze de la turbulence associée à des vitesses moyennes. *Publ. Scien. et Tech. du Ministère de l'Air* no. 345.

DEISSLER, R. G. 1962 Turbulent heat transfer and temperature fluctuations in a field with uniform velocity and temperature gradients. *Int. J. Heat and Mass Trans.* **6**, 257.

FULACHIER, L. & DUMAS, R. 1976 Spectral analogy between temperature and velocity fluctuations in a turbulent boundary layer. *J. Fluid Mech.* **77**, 257.

GEE, J. H. & DAVIES, D. R. 1964 A further note on horizontal dispersion from an instantaneous ground source. *Quart. J. Roy. Met. Soc.* **386**, 478.

GRANT, H. L. 1958 The large eddies of turbulent motion. *J. Fluid Mech.* **4**, 149.

HARRIS, V. G., GRAHAM, J. A. & CORRSIN, S. 1977 Further experiments in nearly homogeneous turbulent shear flow. *J. Fluid Mech.* **81**, 657.

HINZE, J. O. 1975 *Turbulence*, 2nd edn. McGraw-Hill.

HØJSTRUP, J., RASMUSSEN, K. & LARSEN, S. E. 1976 Dynamic calibration of temperature wires in still air. *DISA Info.* **20**, 22.

HWANG, W. S. 1971 Experimental investigation of turbulent shear flows. Ph.D. dissertation, Univ. of Virginia.

JOHNSON, D. S. 1957 Velocity, temperature, and heat-transfer measurements in a turbulent boundary layer downstream of a stepwise discontinuity in wall temperature. *Trans. A.S.M.E. E, J. Appl. Mech.* **24**, 2.

JOHNSON, D. S. 1959 Velocity and temperature fluctuation measurements in a turbulent boundary layer downstream of a stepwise discontinuity in wall temperature. *Trans. A.S.M.E. E, J. Appl. Mech.* **26**, 325.

KAMPÉ DE FÉRIET, J. M. 1937 Sur les équations de la diffusion thermique par turbulence. *Ann. Soc. Sci. Bruxelles I* **57**, 67.

KÁRMÁN, T. VON 1937 The fundamentals of the statistical theory of turbulence. *J. Aero. Sci.* **4**, 131.

KÁRMÁN, T. VON & HOWARTH, L. 1938 On the statistical theory of isotropic turbulence. *Proc. Roy. Soc. A* **164**, 192.

LARUE, J. C., DEATON, T. & GIBSON, C. H. 1975 Measurement of high-frequency turbulent temperature. *Rev. Sci. Instrum.* **46**, 757.

LAUFER, J. 1954 The structure of turbulence in fully developed pipe flow. *NACA Rep.* 1174.

MESTAYER, P. & CHAMBAUD, P. 1979 Some limitations to measurements of turbulence micro-structure with hot and cold wires. *Boundary Layer Met.* **16**, 311.

MULHEARN, P. J. & LUXTON, R. E. 1970 Experiments on uniformly sheared turbulence to large total strains. Charles Kolling Res. Lab., Univ. of Sydney, Rep. TNF-19.

MULHEARN, P. J. & LUXTON, R. E. 1975 The development of turbulence structure in a uniform shear flow. *J. Fluid Mech.* **68**, 577.

REIS, F. B. 1952 Studies of correlation and spectra in homogeneous turbulence. Ph.D. dissertation, Massachusetts Institute of Technology.

REYNOLDS, O. 1894 On the dynamical theory of incompressible fluids and the determination of the criterion. *Phil. Trans. Roy. Soc.* **186**, 123.

ROBERTSON, J. M. 1959 On turbulent plate Couette flow. *Proc. Midwest Conf. Fluid Mech., Univ. Texas, Austin*, p. 169.

ROBERTSON, J. M. & JOHNSON, H. F. 1970 Turbulence structure in plane Couette flow. *J. Eng. Mech. Div., Proc. A.S.C.E.* **96** (EM6), 1171.

ROSE, W. G. 1966 Results of an attempt to generate a homogeneous turbulent shear flow. *J. Fluid Mech.* **25**, 97.

ROSE, W. G. 1970 Interaction of grid turbulence with a uniform mean shear. *J. Fluid Mech.* **44**, 767.

SCHWARZ, W. H. & HOELSCHER, H. E. 1956 Mass transfer in a wetted-wall column: turbulent flow. *A.I.Ch.E. J.* **2**, 101.

SHLIEN, D. J. & CORRSIN, S. 1974 A measurement of Lagrangian velocity autocorrelation in approximately isotropic turbulence. *J. Fluid Mech.* **62**, 255.

SREENIVASAN, K. R., ANTONIA, R. A. & DANH, H. Q. 1977 Temperature dissipation fluctuations in a turbulent boundary layer. *Phys. Fluids* **20**, 1238.

SREENIVASAN, K. R., TAVOULARIS, S., HENRY, R. & CORRSIN, S. 1980 Temperature fluctuations and scales in grid-generated turbulence. *J. Fluid Mech.* **100**, 597–621.

TAVOULARIS, S. 1978*a* A circuit for the measurement of instantaneous temperature in heated turbulent flows. *J. Sci. Instrum.* **11**, 21.

TAVOULARIS, S. 1978*b* Experiments in turbulent transport and mixing, Ph.D. dissertation, Johns Hopkins University.

TENNEKES, H. & LUMLEY, J. L. 1973 *A First Course in Turbulence.* Massachusetts Institute of Technology Press.

TOWNSEND, A. A. 1954 *Q. J. Mech. Appl. Math.* **7**, 104.

UEDA, H. & HINZE, J. O. 1975 Fine-structure turbulence in the wall region of a turbulent boundary layer. *J. Fluid Mech.* **67**, 125.

VENKATARAMANI, K. S. & CHEVRAY, R. 1978 Statistical features of heat transport in grid-generated turbulence: constant gradient case. *J. Fluid Mech.* **86**, 513.

WISKIND, H. K. 1962 A uniform gradient turbulent transport experiment. *J. Geo. Res.* **67**, 3033.

WYNGAARD, J. C. 1968 Measurement of small-scale turbulence structure with hot-wires. *J. Sci. Instrum.* **1**, 1105.

WYNGAARD, J. C. 1969 Spatial resolution of the vorticity meter and other hot-wire arrays. *J. Sci. Instrum.* **2**, 983.

WYNGAARD, J. C. 1971 Spatial resolution of a resistance wire temperature sensor. *Phys. Fluids* **14**, 2052.

YAGLOM, A. M. 1969 Horizontal turbulent transport of heat in the atmosphere and the form of the eddy diffusivity tensor. *Fluid Dyn. Trans.* **4**, 801. Inst. Fund. Techn. Res., Polish Acad. Sci., Warsaw.